

Bounding and Estimating the Classical Information Rate of Quantum Channels with Memory

Michael X. Cao, *Student Member, IEEE*, and Pascal O. Vontobel, *Senior Member, IEEE*

Abstract—We consider the scenario of classical communication over a finite-dimensional quantum channel with memory using separable-state input ensemble and local output measurements. We propose algorithms for estimating and bounding the information rate of such communication setups. Some of the algorithms are extensions of their counterparts for (classical) finite-state-machine channels. Notably, we discuss suitable graphical models for doing the relevant computations. Moreover, the auxiliary channels are learned in a data-driven approach, *i.e.*, only input/output sequences of the true channel are needed, but not the channel model of the true channel.

Index Terms—Quantum Channel, Memory, Information Rate, Bounds

I. INTRODUCTION

WE consider the transmission rate of classical information over a finite-dimensional quantum channel with memory [2], [3], [4]. Given an input system A and an output system B , described by some Hilbert spaces \mathcal{H}_A and \mathcal{H}_B , respectively, a quantum channel can be modeled as a *completely-positive trace preserving* (CPTP) map from the set of density operators on \mathcal{H}_A to the set of density operators on \mathcal{H}_B [5], [6]. Such a quantum channel is said to be finite-dimensional if both \mathcal{H}_A and \mathcal{H}_B are of finite dimension. A *quantum channel with memory* is a quantum channel equipped with a recursive memory system S ; namely it is a CPTP map from the set of density operators on $\mathcal{H}_S \otimes \mathcal{H}_A$ to the set of density operators on $\mathcal{H}_S \otimes \mathcal{H}_B$, where \mathcal{H}_S is the Hilbert space describing S , and \otimes stands for the tensor product. The system S can be understood either as a state of the channel (as illustrated in Fig. 1a), or as a part of the environment that does not decay between consecutive channel uses (as illustrated in Fig. 1b). Interesting examples of quantum channels with memory include the spin chain [7] and fiber optic links [8].

Classical communication over such channels is accomplished by encoding classical data into some density operators before the transmission and applying measurements at the outputs of the channel [5], [6]. In the most generic case, a joint input ensemble and a joint output measurement across multiple channels can be used for encoding and decoding respectively. The scenario involving a k -channel input ensemble and a k -channel output measurement is depicted in Fig. 2, where

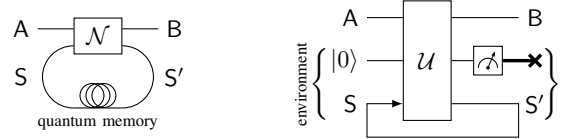
M. X. Cao is with the Department of Information Engineering, The Chinese University of Hong Kong, Shatin, N.T., Hong Kong. E-mail: m.x.cao@iee.org.

P. O. Vontobel is with the Department of Information Engineering and the Institute of Theoretical Computer Science and Communications, The Chinese University of Hong Kong. Email: pascal.vontobel@iee.org.

Supported in part by RGC GRF grants 2150965 and 2151013.

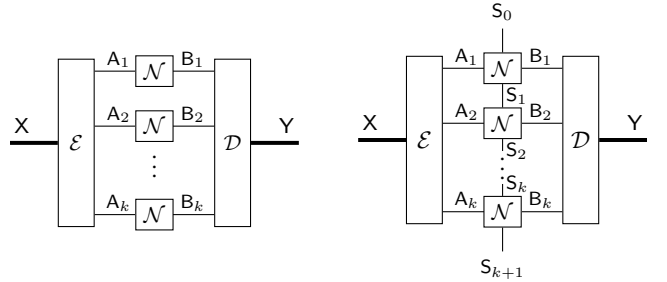
This paper was presented in part at the IEEE Int. Symp. Inf. Theory (ISIT), Aachen, Germany, July 2017 [1].

Submitted. Date of current version: March 4, 2019.



(a) Memory as the state of the channel (b) Memory as undecayed partial environment

Fig. 1: Interpretations of quantum channels with memory.



(a) Memoryless channel (b) Channel with memory

Fig. 2: Classical communications over quantum channels.

- the encoding process \mathcal{E} is described by some ensemble $\{P_X(x), \rho_{A_1}^{(x)}\}_{x \in \mathcal{X}}$ on the joint input system (A_1, \dots, A_k) , with \mathcal{X} being the input alphabet, and $P_X(x)$ being the input distribution;
- the decoding process \mathcal{D} is described by some positive-operator valued measurement (POVM) $\{\Lambda_{B_k}^{(y)}\}_{y \in \mathcal{Y}}$ on the joint output system (B_1, \dots, B_k) , with \mathcal{Y} being the output alphabet;
- the classical input and output are represented by some random variables X and Y , respectively.

The above arrangement straightforwardly results in a (classical) channel from X to Y , whose rate of transmission is given by

$$\mathbf{I}(\mathcal{E}, \mathcal{N}^{\otimes k}, \mathcal{D}) = \limsup_{n \rightarrow \infty} \frac{1}{k \cdot n} \mathbf{I}(X_1^n; Y_1^n). \quad (1)$$

Here, \mathbf{I} stands for the mutual information. As a fundamental result, this quantity can be simplified to $\mathbf{I}(X; Y)$ for the memoryless case [9], [10]. Optimizing $\mathbf{I}(\mathcal{E}, \mathcal{N}^{\otimes k}, \mathcal{D})$ over \mathcal{E} and \mathcal{D} (with $k \rightarrow \infty$) yields the classical capacity of the quantum channel \mathcal{N} , namely

$$C(\mathcal{N}) = \limsup_k \frac{1}{k} \sup_{\mathcal{E}, \mathcal{D}} \mathbf{I}(\mathcal{E}, \mathcal{N}^{\otimes k}, \mathcal{D}). \quad (2)$$

In this paper, we are interested in computing and bounding the information rate as in (1) for finite-dimensional quantum

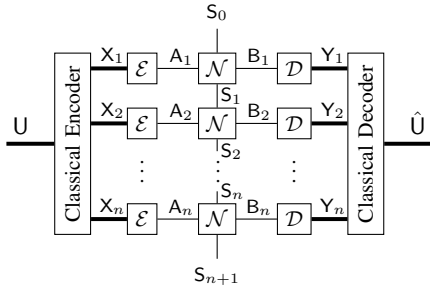


Fig. 3: Classical communication over a quantum channel with memory using a separable ensemble and local measurements.

channels with memory using only separable input ensembles and local output measurements, *i.e.*, the case $k = 1$, which is depicted in Fig. 3. This restriction is equivalent to the scenario where no quantum computing device is present at the sending or receiving end; or the scenario where our manipulation of the channel is limited to a single-channel use. The difficulty of the problem lies with the presence of the quantum memory. In the simplest situation, the memory system exhibits classical properties under certain ensembles and measurements. In this case, the resulting classical communication setup is equivalent to a finite-state-machine channel (FSMC) [11]. The information rate of an FSMC is nontrivial, but can be estimated and bounded efficiently [12], [13].

Our work is highly inspired by [12], where the authors considered the information rate of FSMCs. In particular, for an indecomposable FSMC [11] with channel law W , its information rate is given by

$$\mathbf{I}(Q, W) = \lim_{n \rightarrow \infty} \frac{1}{n} \mathbf{I}(X_1^n; Y_1^n), \quad (3)$$

where $X_1^n = (X_1, \dots, X_n)$ is the channel input process characterized by some sequence of distributions $\{Q^{(n)}\}_n$, and where $Y_1^n = (Y_1, \dots, Y_n)$ is the channel output process. Although, except for very special cases, there are no single-letter or other simple expressions for information rates available, efficient stochastic techniques have been developed for estimating the information rate for *stationary* and *ergodic* input processes $\{Q^{(n)}\}_n$ [12], [14], [15]. (For these techniques, under mild conditions, the numerical estimate of the information rate converges with probability one to the true value when the length of the channel input sequence goes to infinity.) In this paper, we extend such techniques to quantum channels with memory; in particular, we use similar (but extended) graphical models, namely *factor graphs* for quantum probabilities [16] for estimating quantities of interest.

Our work is also partially inspired by [13], where the authors proposed upper and lower bounds based on some so-called auxiliary FSMCs, which are often lower-complexity approximations of the original FSMC. They also provided efficient methods for optimizing these bounds. Such techniques have been proven useful for FSMCs with large state spaces, when the above-mentioned information rate estimation techniques can be overly time-consuming. Interestingly enough, the lower bounds represent achievable rates under mismatched

decoding, where the decoder bases its computations not on the true FSMC but on the auxiliary FSMC [17]. (See the paper [13] for a more detailed discussion of this topic and for further references.) In this paper, we also consider auxiliary channels and their induced bounds. However, the auxiliary channels of our interest take on a larger domain called *quantum-state channels*, which will be defined in Section III. We also propose a method in optimizing these bounds. In particular, our method for optimizing the lower bound is also “data-driven”, in the sense that only the input/output sequences of the original channel are needed, but not the channel model of the original channel.

One must note that even if we can efficiently compute or bound the information rate, it is still a long way to go to compute the classical capacity of a quantum channel with memory. On the one hand, maximizing $\mathbf{I}(\mathcal{E}, \mathcal{N}, \mathcal{D})$ is a difficult problem. (The analogous classical problems have been addressed in [18], [19], and [20].) On the other hand, due to the superadditivity property [21] of quantum channels, which is much more common for quantum channels with memory [22], [23], [24], it is inevitable to consider multi-channel ensembles and measurements.

The rest of this paper is organized as follows. Section II reviews the method of estimating the information rate of an FSMC. Section III models the classical communication scheme over a quantum channel with memory, and defines the notion of quantum-state channels as an equivalent description. A graphical notation in representing such channels is also presented in this section. Section IV estimates the information rate of such channels. Section V considers the upper and lower bounds induced by auxiliary quantum-state channels, and presents methods for optimizing them. Section VI contains numerical examples. Section VII concludes the paper.

A. Further references

In the following, we assume that the reader is familiar with the basic elements of quantum information theory (see [5] or [6] for an introduction). For a general introduction to quantum channels with memory, we refer to the papers by Kretschmann and Werner [3] and by Caruso *et al.* [4].

Moreover, some familiarity with graphical models (like factor graphs) [25], [26], [27] and with techniques for estimating the information rate of an FSMC as presented in [12], [13] will be beneficial. Recall that graphical models are a popular approach for representing multivariate functions with non-trivial factorizations and for doing computations like marginalization [25], [26], [27]. In particular, graphical models can be used to represent joint probability mass functions (pmfs) / probability density functions (pdfs). In the present paper we will heavily rely on the paper [16], which discussed an approach for using normal factor graphs (NFGs) for representing functions that typically appear when doing computations w.r.t. some quantum systems. Alternatively, we could also have used the slightly more compact double-edge normal factor graphs (DE-NFGs) [28]. Probabilities of interest are then obtained by suitably applying the sum-product algorithm or closing-the-box operations.

B. Notations

We use the following conventions throughout the paper:

- Vectors are denoted using boldface letters.
- Sans-serif letters are being used to denote either random variables or quantum systems.
- Upper and lower indices are used as the starting and ending indices, respectively, of the elements in a vector or an ordered collections of random variables or quantum systems. For example,
 - $\mathbf{x}_1^n \equiv (x_1, x_2, \dots, x_n)$ denotes an n -tuple with elements x_1 up to x_n ;
 - $\mathbf{X}_1^n \equiv (X_1, X_2, \dots, X_n)$ denotes a sequence of random variables;
 - $\mathbf{S}_0^n \equiv (S_0, S_1, \dots, S_n)$ denotes the collective quantum system consisting of subsystems S_0 up to S_n .
- The set of all density operators over a Hilbert space \mathcal{H} is denoted by $\mathfrak{D}(\mathcal{H})$; its elements are represented using Greek letters, *e.g.*, ρ_S denotes a density operator of some quantum system S .

As it should be clear from the context, we also overload the symbol \mathbf{H} to denote either the Shannon entropy or the von Neumann entropy, and the symbol \mathbf{I} to denote either the classical or quantum mutual information.

II. REVIEW ON FINITE-STATE MACHINE CHANNELS: INFORMATION RATE, ITS ESTIMATION, AND BOUNDS

In this section, we review the methods developed in [12] for estimating the information rate of an (classical) FSMC, and the auxiliary-channel-induced upper and lower bounds studied in [13]. As we will see, the development in later sections about quantum channels will have many similarities, but also some important differences.

A. Finite-State Machine Channels (FSMCs) and their Graphical Representation

A (time-invariant) finite-state machine channel (FSMC) consists of an input alphabet \mathcal{X} , an output alphabet \mathcal{Y} , a state alphabet \mathcal{S} , all of which are finite, and a channel law $W(y, s' | x, s)$, where the latter equals the probability of receiving $y \in \mathcal{Y}$ and ending up in state $s' \in \mathcal{S}$ given channel input $x \in \mathcal{X}$ and previous channel state $s \in \mathcal{S}$. The relationship among the input, output, and state processes $\mathbf{X}_1^n, \mathbf{Y}_1^n, \mathbf{S}_0^n$ of n -channel uses can be described by the conditional pmf

$$W(\mathbf{y}_1^n, \mathbf{s}_1^n | \mathbf{x}_1^n, s_0) \triangleq P_{\mathbf{Y}_1^n, \mathbf{S}_1^n | \mathbf{X}_1^n, S_0}(\mathbf{y}_1^n, \mathbf{s}_1^n | \mathbf{x}_1^n, s_0), \quad (4)$$

$$= \prod_{\ell=1}^n W(y_\ell, s_\ell | x_\ell, s_{\ell-1}), \quad (5)$$

where $x_\ell \in \mathcal{X}$, $y_\ell \in \mathcal{Y}$, and $s_\ell \in \mathcal{S}$ for each ℓ .

Example 1 (Gilbert–Elliott channels). A notable class of examples of FSMCs are the Gilbert–Elliott channels [29], which can be either in the so-called “good” state or in the so-called “bad” state. If the channel is in the “good” state, then it behaves like a binary symmetric channel (BSC) with cross-over probability p_g , but if the channel is in the “bad” state, then it behaves like a BSC with cross-over probability p_b , where

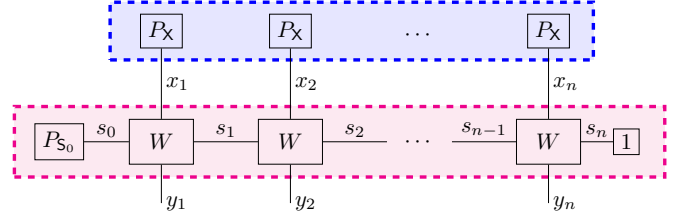


Fig. 4: Channel with a classical state: Closing the cyan box yields the the input process $\{Q^{(n)}\}_n$, closing the magenta box yields the joint channel law $W(\mathbf{y}_1^n | \mathbf{x}_1^n)$.

usually $|p_b - \frac{1}{2}| < |p_g - \frac{1}{2}|$. The state process itself is a first-order stationary ergodic Markov process that is independent of the input process.¹ (For more details, see, *e.g.*, the discussions in [13].) \square

Given an input process $\{Q^{(n)}\}_n$ and an initial state pmf $P_{S_0}(s_0)$, we can write down the joint pmf of $(\mathbf{X}_1^n, \mathbf{Y}_1^n, \mathbf{S}_0^n)$ as

$$\begin{aligned} g(\mathbf{x}_1^n, \mathbf{y}_1^n, \mathbf{s}_0^n) &\triangleq P_{\mathbf{X}_1^n, \mathbf{Y}_1^n, \mathbf{S}_0^n}(\mathbf{x}_1^n, \mathbf{y}_1^n, \mathbf{s}_0^n) \\ &= P_{S_0}(s_0) \cdot Q^{(n)}(\mathbf{x}_1^n) \cdot \prod_{\ell=1}^n W(y_\ell, s_\ell | x_\ell, s_{\ell-1}). \end{aligned} \quad (6)$$

The factorization of $g(\mathbf{x}_1^n, \mathbf{y}_1^n, \mathbf{s}_0^n)$ as shown in (7) can be visualized with the help of a normal factor graph (NFG) as in Fig. 4. In this context, $g(\mathbf{x}_1^n, \mathbf{y}_1^n, \mathbf{s}_0^n)$ is called the global function of the NFG. In particular:

- The part of the NFG inside the magenta box represents $W(\mathbf{y}_1^n, \mathbf{s}_1^n | \mathbf{x}_1^n, s_0)$, *i.e.*, the probability of obtaining \mathbf{y}_1^n and \mathbf{s}_1^n given \mathbf{x}_1^n and s_0 . After applying the *closing-the-box operation*, *i.e.*, after summing over all the variables associated with edges completely inside the red box, we obtain the joint channel law $W(\mathbf{y}_1^n | \mathbf{x}_1^n) \triangleq \sum_{\mathbf{s}_0^n} P_{S_0}(s_0) \cdot W(\mathbf{y}_1^n, \mathbf{s}_1^n | \mathbf{x}_1^n, s_0)$.
- The part of the NFG inside the cyan box represents the input process $Q^{(n)}(\mathbf{x}_1^n)$. Here, for simplicity, the input process is an i.i.d. process characterized by the pmf Q , *i.e.*, $Q^{(n)}(\mathbf{x}_1^n) = \prod_{\ell=1}^n Q(x_\ell)$.
- The function $g(\mathbf{x}_1^n, \mathbf{y}_1^n) \triangleq \sum_{\mathbf{s}_0^n} g(\mathbf{x}_1^n, \mathbf{y}_1^n, \mathbf{s}_0^n)$, which is obtained by summing the global function $g(\mathbf{x}_1^n, \mathbf{y}_1^n, \mathbf{s}_0^n)$ over \mathbf{s}_0^n , represents the corresponding marginal pmf over \mathbf{x}_1^n and \mathbf{y}_1^n . The function $g(\mathbf{s}_0^n) \triangleq \sum_{\mathbf{x}_1^n, \mathbf{y}_1^n} g(\mathbf{x}_1^n, \mathbf{y}_1^n, \mathbf{s}_0^n)$, which is obtained by summing the global function over \mathbf{x}_1^n and \mathbf{y}_1^n , represents the corresponding marginal pmf over s . Other marginal pmfs can be obtained similarly.

Equipped with the notion of the closing-the-box operation (see item a) above), such NFG representations can be useful in computing a number of quantities of interests. For example, to prove that (5) is indeed a valid conditional pmf, it suffices to show that

$$\sum_{\mathbf{s}_1^n, \mathbf{y}_1^n} W(\mathbf{y}_1^n, \mathbf{s}_1^n | \tilde{\mathbf{x}}_1^n, \tilde{s}_0) = 1 \quad \forall \tilde{\mathbf{x}}_1^n \in \mathcal{X}^{\otimes n}, \tilde{s}_0 \in \mathcal{S}, \quad (8)$$

¹The independence of the state process on the input process is a particular feature of the Gilbert–Elliott channel. In general, the state process of a finite-state channel can depend on the input process.

which can be verified via a sequence of closing-the-box operations as in Fig. 14 in the Appendix. Such techniques are at the heart of the information-rate-estimation methods as in [12]. The details are reviewed in the next subsection.

B. Information Rate Estimation

The approach of [12] for estimating information rates of FSMCs, as reviewed in this section, is based on the Shannon–McMillan–Breiman theorem (see, *e.g.*, [10]) and suitable generalizations. We make the following assumptions.

- As already mentioned, the derivations in this paper are for the case where the input process $\mathbf{X} = (\mathbf{X}_1, \mathbf{X}_2, \dots)$ is an i.i.d. process. The results can be generalized to other stationary ergodic input processes that can be represented by a finite-state-machine source (FSMS). Technically, this is done by defining a new state that combines the source state and the channel state.
- We assume that the FSMC is indecomposable, which roughly means that in the long term the behavior of the channel is independent of the initial channel state distribution P_{S_0} (see [11] for the exact definition). For such channels and stationary ergodic input processes, the information rate I in (3) is well defined.

Let $W(\mathbf{y}_1^n | \mathbf{x}_1^n)$ be the joint channel law of an FSMC satisfying the assumptions above. As aforementioned, the information rate of such a channel using the i.i.d. input distribution $\{Q^{(n)} \equiv Q^{\otimes n}\}_n$ is given by (3), *i.e.*, by

$$I(Q, W) = \lim_{n \rightarrow \infty} \frac{1}{n} \mathbf{I}(\mathbf{X}_1^n; \mathbf{Y}_1^n), \quad (3')$$

where the input process \mathbf{X}_1^n and the output process \mathbf{Y}_1^n are jointly distributed according to

$$P_{\mathbf{X}_1^n, \mathbf{Y}_1^n}(\mathbf{x}_1^n, \mathbf{y}_1^n) = \prod_{\ell=1}^n Q(x_\ell) \cdot W(\mathbf{y}_1^n | \mathbf{x}_1^n). \quad (9)$$

One can rewrite (3) as

$$I(Q, W) = H(\mathbf{X}) + H(\mathbf{Y}) - H(\mathbf{X}, \mathbf{Y}), \quad (10)$$

where the *entropic rates* $H(\mathbf{X})$, $H(\mathbf{Y})$ and $H(\mathbf{X}, \mathbf{Y})$ are defined as

$$H(\mathbf{X}) \triangleq \lim_{n \rightarrow \infty} \frac{1}{n} \mathbf{H}(\mathbf{X}_1^n), \quad (11)$$

$$H(\mathbf{Y}) \triangleq \lim_{n \rightarrow \infty} \frac{1}{n} \mathbf{H}(\mathbf{Y}_1^n), \quad (12)$$

$$H(\mathbf{X}, \mathbf{Y}) \triangleq \lim_{n \rightarrow \infty} \frac{1}{n} \mathbf{H}(\mathbf{X}_1^n, \mathbf{Y}_1^n). \quad (13)$$

We proceed as in [12]. (For more background information, see the references in [12], in particular [30].) Namely, because of (10) and

$$-\frac{1}{n} \log P(\mathbf{X}_1^n) \xrightarrow{n \rightarrow \infty} H(\mathbf{X}) \quad \text{with probability 1,} \quad (14)$$

$$-\frac{1}{n} \log P(\mathbf{Y}_1^n) \xrightarrow{n \rightarrow \infty} H(\mathbf{Y}) \quad \text{with probability 1,} \quad (15)$$

$$-\frac{1}{n} \log P(\mathbf{X}_1^n, \mathbf{Y}_1^n) \xrightarrow{n \rightarrow \infty} H(\mathbf{X}, \mathbf{Y}) \quad \text{with probability 1,} \quad (16)$$

by choosing some large number n , we have the approximation

$$I(Q, W) \approx -\frac{1}{n} \log P_{\mathbf{X}_1^n}(\tilde{\mathbf{x}}_1^n) - \frac{1}{n} \log P_{\mathbf{Y}_1^n}(\tilde{\mathbf{y}}_1^n) \quad (17) \\ + \frac{1}{n} \log P_{\mathbf{X}_1^n, \mathbf{Y}_1^n}(\tilde{\mathbf{x}}_1^n, \tilde{\mathbf{y}}_1^n),$$

where $\tilde{\mathbf{x}}_1^n$ and $\tilde{\mathbf{y}}_1^n$ are some input and output sequences, respectively, randomly generated according to

$$P_{\mathbf{X}_1^n, \mathbf{Y}_1^n}(\tilde{\mathbf{x}}_1^n, \tilde{\mathbf{y}}_1^n) = \sum_{s_0^n} P_{S_0}(s_0) \cdot Q^{(n)}(\tilde{\mathbf{x}}_1^n) \cdot W(\tilde{\mathbf{y}}_1^n, \mathbf{s}_1^n | \tilde{\mathbf{x}}_1^n, s_0), \quad (18)$$

where $W(\tilde{\mathbf{y}}_1^n, \mathbf{s}_1^n | \tilde{\mathbf{x}}_1^n, s_0)$ is defined in (5). Note that $\tilde{\mathbf{x}}_1^n$ can be obtained by simulating the input process, and $\tilde{\mathbf{y}}_1^n$ can be obtained by simulating the channel for the given input string $\tilde{\mathbf{x}}_1^n$. The latter can be done by keeping track of $P_{\mathbf{Y}_\ell | \mathbf{X}_1^\ell, \mathbf{Y}_1^{\ell-1}}(y_\ell | \tilde{\mathbf{x}}_1^\ell, \tilde{\mathbf{y}}_1^{\ell-1})$, which is proportional to $P_{\mathbf{Y}_\ell, \mathbf{Y}_1^{\ell-1} | \mathbf{X}_1^\ell}(y_\ell, \tilde{\mathbf{y}}_1^{\ell-1} | \tilde{\mathbf{x}}_1^\ell)$, and can be efficiently calculated by applying suitable closing-the-box operations as in Fig. 16 in the Appendix.

We continue by showing how the three terms appearing on the right-hand side of (17) can be computed efficiently. We show it explicitly for the second term, and then outline it for the first and the third term.

In order to efficiently compute the second term on the right-hand side of (17), *i.e.*, $-\frac{1}{n} \log P_{\mathbf{Y}_1^n}(\tilde{\mathbf{y}}_1^n)$, we consider the *state metric* defined in [12] as

$$\mu_\ell^{\mathbf{Y}}(s_\ell) \triangleq \sum_{\mathbf{x}_1^\ell} \sum_{s_0^{\ell-1}} P_{S_0}(s_0) \cdot Q^{(\ell)}(\mathbf{x}_1^\ell) \cdot W(\tilde{\mathbf{y}}_1^\ell, \mathbf{s}_1^\ell | \mathbf{x}_1^\ell, s_0). \quad (19)$$

In this case,

$$P_{\mathbf{Y}_1^n}(\tilde{\mathbf{y}}_1^n) = \sum_{s_n} \mu_n^{\mathbf{Y}}(s_n) \quad (20)$$

and the calculation of $\mu_\ell^{\mathbf{Y}}(s_\ell)$ can be done iteratively as

$$\mu_\ell^{\mathbf{Y}}(s_\ell) \\ = \sum_{x_\ell} \sum_{s_{\ell-1}} \mu_{\ell-1}^{\mathbf{Y}}(s_{\ell-1}) \cdot Q(x_\ell | \mathbf{x}_1^{\ell-1}) \cdot W(\tilde{y}_\ell, s_\ell | x_\ell, s_{\ell-1}) \\ = \sum_{x_\ell} \sum_{s_{\ell-1}} \mu_{\ell-1}^{\mathbf{Y}}(s_{\ell-1}) \cdot Q(x_\ell) \cdot W(\tilde{y}_\ell, s_\ell | x_\ell, s_{\ell-1}). \quad (21)$$

Eq. (21) is visualized in Fig. 18 as applying suitable closing-the-box operations to the NFG in Fig. 4.

However, since the value of $\mu_\ell^{\mathbf{Y}}(s_\ell)$ tends to zero as ℓ grows, such recursive calculations are numerically inconvenient. A solution is to *normalize* $\mu_\ell^{\mathbf{Y}}(s_\ell)$ after each use of (21) and to keep track of the scaling coefficients. Namely,

$$\bar{\mu}_\ell^{\mathbf{Y}}(s_\ell) \triangleq \\ \lambda_\ell^{\mathbf{Y}} \cdot \sum_{x_\ell} \sum_{s_{\ell-1}} \bar{\mu}_{\ell-1}^{\mathbf{Y}}(s_{\ell-1}) \cdot Q(x_\ell) \cdot W(\tilde{y}_\ell, s_\ell | x_\ell, s_{\ell-1}), \quad (22)$$

where the scaling factor $\lambda_\ell^{\mathbf{Y}} > 0$ is chosen such that $\sum_{s_\ell} \bar{\mu}_\ell^{\mathbf{Y}}(s_\ell) = 1$. With this, Eq. (20) can be rewritten as

$$P_{\mathbf{Y}_1^n}(\tilde{\mathbf{y}}_1^n) = \prod_{\ell=1}^n (\lambda_\ell^{\mathbf{Y}})^{-1}. \quad (23)$$

Finally, we arrive at the following efficient procedure for computing $-\frac{1}{n} \log P_{\mathbf{Y}_1^n}(\tilde{\mathbf{y}}_1^n)$:

- For $\ell = 1, \dots, n$, iteratively compute the normalized state metric and with that the scaling factors λ_ℓ^Y .
- Conclude with the result

$$-\frac{1}{n} \log P_{Y_1^n}(\mathbf{y}_1^n) = \frac{1}{n} \sum_{\ell=1}^n \log(\lambda_\ell^Y). \quad (24)$$

The third term on the right-hand side of (17) can be evaluated by an analogous procedure, where the state metric $\mu_\ell^Y(s_\ell)$ is replaced by the state metric

$$\mu_\ell^{XY}(s_\ell) \triangleq \sum_{s_0^{\ell-1}} P_{S_0}(s_0) \cdot Q^{(\ell)}(\check{\mathbf{x}}_1^\ell) \cdot W(\check{\mathbf{y}}_1^\ell, \mathbf{s}_1^\ell | \check{\mathbf{x}}_1^\ell). \quad (25)$$

The iterative calculation of $\mu_\ell^{XY}(s_\ell)$ is visualized in Fig. 20.

Finally, the first term on the right-hand side of (17) can be trivially evaluated if X is an i.i.d. process, and with a similar approach as above if it is described by a finite-state process.

The above discussion is summarized as Algorithm 2.

C. Auxiliary Channels and Bounds on the Information Rate

As already mentioned in Section I, auxiliary channels are introduced when the state space of the FSMC is too large, making the calculation as in Algorithm 2 intractable. More precisely, given an auxiliary forward FSMC (AF-FSMC) $\hat{W}(y_\ell \hat{s}_\ell | x_\ell, \hat{s}_{\ell-1})$ and an auxiliary backward FSMC (AB-FSMC) $\hat{V}(x_\ell, \hat{s}_\ell | y_\ell, \hat{s}_{\ell-1})$, upper and lower bounds of the information rate are given in [12], [13] as

$$\bar{I}^{(n)}(\hat{W}) \triangleq \frac{1}{n} \sum_{\mathbf{x}_1^n, \mathbf{y}_1^n} Q(\mathbf{x}_1^n) W(\mathbf{y}_1^n | \mathbf{x}_1^n) \log \left(\frac{W(\mathbf{y}_1^n | \mathbf{x}_1^n)}{(Q\hat{W})(\mathbf{y}_1^n)} \right), \quad (26)$$

$$\underline{I}^{(n)}(\hat{V}) \triangleq \frac{1}{n} \sum_{\mathbf{x}_1^n, \mathbf{y}_1^n} Q(\mathbf{x}_1^n) W(\mathbf{y}_1^n | \mathbf{x}_1^n) \log \left(\frac{\hat{V}(\mathbf{x}_1^n | \mathbf{y}_1^n)}{Q^{(n)}(\mathbf{x}_1^n)} \right). \quad (27)$$

In particular, given an AF-FSMC \hat{W} , the paper [13] considered the induced AB-FSMC $\hat{V}(\mathbf{x} | \mathbf{y}) \triangleq Q(\mathbf{x}) \hat{W}(\mathbf{y} | \mathbf{x}) / Q\hat{W}(\mathbf{y})$. In this case,

$$\underline{I}^{(n)}(\hat{V}) = \frac{1}{n} \sum_{\mathbf{x}_1^n, \mathbf{y}_1^n} Q^{(n)}(\mathbf{x}_1^n) W(\mathbf{y}_1^n | \mathbf{x}_1^n) \log \left(\frac{\hat{W}(\mathbf{y}_1^n | \mathbf{x}_1^n)}{Q\hat{W}(\mathbf{y}_1^n)} \right). \quad (28)$$

The difference function $\Delta^{(n)}(\hat{W})$ is defined as

$$\Delta^{(n)}(\hat{W}) \triangleq \bar{I}^{(n)}(\hat{W}) - \underline{I}^{(n)}(\hat{V}) \quad (29)$$

$$= \frac{1}{n} \sum_{\mathbf{x}_1^n, \mathbf{y}_1^n} Q(\mathbf{x}_1^n) W(\mathbf{y}_1^n | \mathbf{x}_1^n) \log \left(\frac{W(\mathbf{y}_1^n | \mathbf{x}_1^n)}{\hat{W}(\mathbf{y}_1^n | \mathbf{x}_1^n)} \right) \quad (30)$$

$$= \frac{1}{n} D_{\text{KL}} \left(Q(\mathbf{x}_1^n) W(\mathbf{y}_1^n | \mathbf{x}_1^n) \parallel Q(\mathbf{x}_1^n) \hat{W}(\mathbf{y}_1^n | \mathbf{x}_1^n) \right), \quad (31)$$

where $D_{\text{KL}}(\cdot \parallel \cdot)$ stands for the Kullback–Leibler (KL) divergence. Apparently, $\Delta^{(n)}(\hat{W}) \geq 0$, and equality holds if and only if $\hat{W}(\mathbf{y}_1^n | \mathbf{x}_1^n) = W(\mathbf{y}_1^n | \mathbf{x}_1^n)$ for all \mathbf{x}_1^n and \mathbf{y}_1^n with positive support. An efficient algorithm for finding a local minimum of the difference function was proposed in [13]; We refer to [13] for further detail.

Algorithm 2 Estimating the information rate of an FSMC

Input: indecomposable FSMC channel law W ,
input distribution Q ,
large positive integer n .

Output: $I(Q, W) \approx \mathbf{H}(X) + \hat{\mathbf{H}}(Y) - \hat{\mathbf{H}}(X, Y)$.

- 1: Initialize the channel state distribution P_{S_0} as a uniform distribution over \mathcal{S}
 - 2: Generate an input sequence $\check{\mathbf{x}}_1^n \sim Q^{\otimes n}$
 - 3: Generate a corresponding output sequence $\check{\mathbf{y}}_1^n$
 - 4: $\bar{\mu}_0^Y \leftarrow P_{S_0}$
 - 5: **for each** $\ell = 1, \dots, n$ **do**
 - 6: $\mu_\ell^Y(s_\ell) \leftarrow \sum_{x_\ell, s_{\ell-1}} \bar{\mu}_{\ell-1}^Y(s_{\ell-1}) \cdot Q(x_\ell) \cdot W(\check{y}_\ell, s_\ell | x_\ell, s_{\ell-1})$
 - 7: $\lambda_\ell^Y \leftarrow \sum_{s_\ell} \mu_\ell^Y(s_\ell)$;
 - 8: $\bar{\mu}_\ell^Y \leftarrow \mu_\ell^Y / \lambda_\ell^Y$
 - 9: **end for**
 - 10: $\hat{\mathbf{H}}(Y) \leftarrow -\frac{1}{n} \sum_{\ell=1}^n \log(\lambda_\ell^Y)$
 - 11: $\bar{\mu}_0^{XY} \leftarrow P_{S_0}$
 - 12: **for each** $\ell = 1, \dots, n$ **do**
 - 13: $\mu_\ell^{XY}(s_\ell) \leftarrow \sum_{x_\ell, s_{\ell-1}} \bar{\mu}_{\ell-1}^{XY}(s_{\ell-1}) \cdot Q(\check{x}_\ell) \cdot W(\check{y}_\ell, s_\ell | \check{x}_\ell, s_{\ell-1})$
 - 14: $\lambda_\ell^{XY} \leftarrow \sum_{s_\ell} \mu_\ell^{XY}(s_\ell)$
 - 15: $\bar{\mu}_\ell^{XY} \leftarrow \mu_\ell^{XY} / \lambda_\ell^{XY}$
 - 16: **end for**
 - 17: $\hat{\mathbf{H}}(X, Y) \leftarrow -\frac{1}{n} \sum_{\ell=1}^n \log(\lambda_\ell^{XY})$
 - 18: $\mathbf{H}(X) \leftarrow -\sum_x Q(x) \log Q(x)$
 - 19: Estimate $I(Q, W)$ as $\mathbf{H}(X) + \hat{\mathbf{H}}(Y) - \hat{\mathbf{H}}(X, Y)$.
-

III. QUANTUM CHANNEL WITH MEMORY AND THEIR GRAPHICAL REPRESENTATION

In this section, we formalize our notations and modeling of quantum channels with memory [2], [3], [4] and of classical communications over such channels. In particular, we will define a class of channels named “quantum-state channels”, which is an alternative description of the classical communications over quantum channels with memory. In addition, we will introduce several NFGs for representing these channels and processes.

A. Classical communications over a quantum channel with memory

As already mentioned in Section I, a quantum channel with memory is a completely-positive trace preserving (CPTP) map

$$\mathcal{N} : \mathfrak{D}(\mathcal{H}_S \otimes \mathcal{H}_A) \rightarrow \mathfrak{D}(\mathcal{H}_{S'} \otimes \mathcal{H}_A), \quad (32)$$

where A is the input system, B is the output system, S and S' are, respectively, the memory systems before and after the channel use. The Hilbert spaces \mathcal{H}_A , \mathcal{H}_B , and $\mathcal{H}_S \equiv \mathcal{H}_{S'}$ are the state spaces corresponding to those systems.

In the present paper, we consider classical communication over such channels using some separable input ensemble and local output measurements; namely, the encoder and decoder are, respectively, some classical-to-quantum and quantum-to-classical channels involving a single input or output system. In particular, given an ensemble $\{\rho_A^{(x)}\}_{x \in \mathcal{X}}$ and a measurement

$\{\Lambda_B^{(y)}\}_{y \in \mathcal{Y}}$, we define the encoding and decoding function, respectively, as

$$\text{Encoding } \mathcal{E} : \mathfrak{P}(\mathcal{X}) \rightarrow \mathfrak{D}(\mathcal{H}_A) \quad (33)$$

$$p_X \mapsto \sum_{x \in \mathcal{X}} p_X(x) \rho_A^{(x)}, \quad (34)$$

$$\text{Decoding } \mathcal{D} : \mathfrak{D}(\mathcal{H}_B) \rightarrow \mathfrak{P}(\mathcal{Y}) \quad (35)$$

$$\sigma_B \mapsto p_Y, \quad (36)$$

where $\mathfrak{P}(\mathcal{Y})$ is the set of pmfs over \mathcal{Y} , where \mathfrak{D} stands for the space of density operators as mentioned at the end of Section I, and where p_Y in (36) is defined as $p_Y(y) \triangleq \text{tr}(\Lambda_B^{(y)} \cdot \sigma_B)$. We emphasize that in our setup, the ensemble $\{\rho_A^{(x)}\}_{x \in \mathcal{X}}$ and measurements $\{\Lambda_B^{(y)}\}_{y \in \mathcal{Y}}$ are given and fixed. Furthermore, we assume that one does not have access to the memory systems of the channel. In this case, the memory system S before each channel use shall be independent of the input system A, namely, the joint memory-input operator shall take the form of $\rho_S \otimes \rho_A$ at each channel input.

With this, the probability of receiving $y \in \mathcal{Y}$, given that $x \in \mathcal{X}$ was sent and given that the density operator of the memory system *before* the usage of the channel was ρ_S , equals

$$P_{Y|X;S}(y|x; \rho_S) = \text{tr} \left(\Lambda_B^{(y)} \cdot \text{tr}_S \mathcal{N}(\rho_A^{(x)} \otimes \rho_S) \right), \quad (37)$$

which can also be written as

$$P_{Y|X;S}(y|x; \rho_S) = \text{tr} \left((I \otimes \Lambda_B^{(y)}) \cdot \mathcal{N}(\rho_A^{(x)} \otimes \rho_S) \right), \quad (38)$$

where tr_S stands for the *partial trace* operator that extracts the subsystem B from the joint system (S'B).² Moreover, assuming that y was observed, the the density operator of the memory system *after* the channel use is given by

$$\rho_{S'} = \frac{\text{tr}_B \left((I \otimes \Lambda_B^{(y)}) \cdot \mathcal{N}(\rho_A^{(x)} \otimes \rho_S) \right)}{\text{tr} \left((I \otimes \Lambda_B^{(y)}) \cdot \mathcal{N}(\rho_A^{(x)} \otimes \rho_S) \right)}. \quad (39)$$

Notice that the denominator in (39) equals the expressions in (37) and (38). One should note that, though the input and the memory systems are inherently independent before each channel use, the output and the memory systems after each channel use can be correlated or even entangled. In particular, this translates to the fact that the decoding outcome y can have an influence on the memory system as indicated in (39).

Consider using the channel n times consecutively with the above scheme. The joint channel law, namely the conditional pmf of the channel outputs Y_1^n given the channel inputs X_1^n and the initial channel state ρ_{S_0} , can be computed iteratively using (38) and (39). In particular, the joint conditional pmf can be computed as

$$P_{Y_1^n | X_1^n; S_0}(y_1^n | x_1^n; \rho_{S_0}) = \prod_{\ell=1}^n P_{Y_\ell | X_\ell; S_{\ell-1}}(y_\ell | x_\ell; \rho_{S_{\ell-1}}), \quad (40)$$

²The definition of partial trace can be found in multiple sources. For example, we refer to [5, Section 2.4.3].

where we compute the density operators $\{\rho_{S_\ell}\}_{\ell=1}^n$ iteratively using (39) as

$$\rho_{S_\ell} = \frac{\text{tr}_B \left((I \otimes \Lambda_B^{(y_\ell)}) \cdot \mathcal{N}(\rho_A^{(x_\ell)} \otimes \rho_{S_{\ell-1}}) \right)}{\text{tr} \left((I \otimes \Lambda_B^{(y_\ell)}) \cdot \mathcal{N}(\rho_A^{(x_\ell)} \otimes \rho_{S_{\ell-1}}) \right)}. \quad (41)$$

B. Quantum-State Channels

For each channel-ensemble-measurement configuration $(\mathcal{N}, \{\rho_A^{(x)}\}_{x \in \mathcal{X}}, \{\Lambda_B^{(y)}\}_{y \in \mathcal{Y}})$ as introduced above, one ends up with a joint conditional pmf, as in (40). However, this relationship is not bijective. In particular, consider unitary operators U_A and U_B acting on \mathcal{H}_A and \mathcal{H}_B , respectively. The following configuration induces exactly the same joint conditional pmf:

$$\begin{aligned} \tilde{\mathcal{N}} : \tilde{\rho}_{SA} &\mapsto (I_S \otimes U_B) \left(\mathcal{N} \left((I_S \otimes U_A) \tilde{\rho}_{SA} (I_S \otimes U_A^H) \right) \right) (I_S \otimes U_B^H), \\ \tilde{\rho}_A^{(x)} &\triangleq U_A^H \cdot \rho_A^{(x)} \cdot U_A \quad \forall x \in \mathcal{X}, \\ \tilde{\Lambda}_B^{(y)} &\triangleq U_B^H \cdot \Lambda_B^{(y)} \cdot U_B \quad \forall y \in \mathcal{Y}. \end{aligned}$$

Such redundancy is not only tedious, but also detrimental when we try to compare different channels; in particular, when we try to introduce proper auxiliary channels to approximate the original communication scheme.

In this subsection, we introduce a class of channels called *quantum-state channels* to eliminate such redundancies. In particular, notice that the statistical behavior of the aforementioned communication scheme is fully specified via (38) and (39); which are in turn determined by the group of completely positive mappings $\{\mathcal{N}^{y|x}\}_{x \in \mathcal{X}, y \in \mathcal{Y}}$ defined as

$$\mathcal{N}^{y|x} : \rho_S \mapsto \text{tr}_B \left((I \otimes \Lambda_B^{(y)}) \cdot \mathcal{N}(\rho_A^{(x)} \otimes \rho_S) \right). \quad (42)$$

In this case, (38), (39), and (40) can be rewritten, respectively, as

$$P_{Y|X;S}(y|x; \rho_S) = \text{tr} \left(\mathcal{N}^{y|x}(\rho_S) \right), \quad (43)$$

$$\rho_{S'} = \mathcal{N}^{y|x}(\rho_S) / \text{tr} \left(\mathcal{N}^{y|x}(\rho_S) \right), \quad (44)$$

$$P_{Y_1^n | X_1^n; S_0}(y_1^n | x_1^n; \rho_{S_0}) = \text{tr} \left(\mathcal{N}^{y_n | x_n} \circ \dots \circ \mathcal{N}^{y_1 | x_1}(\rho_{S_0}) \right). \quad (45)$$

Thus, the operators $\{\mathcal{N}^{y|x}\}_{x \in \mathcal{X}, y \in \mathcal{Y}}$ fully specify the joint conditional pmf as in (45). Moreover, such specification is also *unique*; namely, any two sets of channel-ensemble-measurement configurations shall end up with the same joint channel law if and only if the mappings defined in (42) are identical. This inspires us to make the following definition.

Definition 3 (Quantum-State Channel). A (finite) class of completely-positive operators $\{\mathcal{N}^{y|x}\}_{x \in \mathcal{X}, y \in \mathcal{Y}}$ (acting on the same Hilbert space) is said to be a (classical-input classical output) *quantum-state channel* (CC-QSC) if $\sum_{y \in \mathcal{Y}} \mathcal{N}^{y|x}$ is trace-preserving for each $x \in \mathcal{X}$. \square

Given any channel-ensemble-measurement configuration as described in Section III-A, one can always define a corresponding CC-QSC by (42). On the other hand, as stated in the proposition below, the converse is also true.

Proposition 4. *Given CC-QSC $\{\mathcal{N}^{y|x}\}_{x \in \mathcal{X}, y \in \mathcal{Y}}$, there exists some quantum channel with memory \mathcal{N} as in (32) such that (42) holds with ensemble $\{\rho_A^{(x)} = |x\rangle\langle x|\}_{x \in \mathcal{X}}$ and*

measurement $\{\Lambda_B^{(y)} = |y\rangle\langle y|\}_{y \in \mathcal{Y}}$. Here, \mathcal{H}_A and \mathcal{H}_B are defined such that $\{|x\rangle\}_x$ and $\{|y\rangle\}_y$ are orthonormal bases of \mathcal{H}_A and \mathcal{H}_B , respectively.

Proof. It suffices to show that there exists a CPTP map \mathcal{N} such that for all $\rho_S \in \mathfrak{D}(\mathcal{H}_S)$, and $x \in \mathcal{X}$,

$$\mathcal{N} : \rho_S \otimes |x\rangle\langle x| \mapsto \sum_{y \in \mathcal{Y}} \mathcal{N}^{y|x}(\rho_S) \otimes |y\rangle\langle y|.$$

By convex-linearity of CPTP maps, such an \mathcal{N} can be constructed by specifying

$$\mathcal{N}(|s\rangle\langle s| \otimes |x\rangle\langle x|) \triangleq \sum_{y \in \mathcal{Y}} \mathcal{N}^{y|x}(|s\rangle\langle s|) \otimes |y\rangle\langle y|,$$

for each $x \in \mathcal{X}$, $s \in \mathcal{S}$, and where $\{|s\rangle\}_{s \in \mathcal{S}}$ is some orthonormal basis of \mathcal{H}_S . \square

C. Visualization using Normal Factor Graphs

In this subsection, we focus on the computations of (43), (44), and (45) for the situation where the involved channel \mathcal{N} is of finite dimension. In analogy to the FSMCs, we demonstrate how to use NFGs to facilitate and visualize the relevant computations. Our use of NFGs for describing quantum systems follows [16].

By Proposition 4, let us consider a CC-QSC $\{\mathcal{N}^{y|x}\}_{x \in \mathcal{X}, y \in \mathcal{Y}}$ acting on \mathcal{H}_S , where $d = \dim(\mathcal{H}_S)$ is finite, and $\{|s\rangle\}_{s \in \mathcal{S}}$ is an orthonormal basis of \mathcal{H}_S . (Apparently, $|\mathcal{S}| = d$.) Since for each x and y , $\mathcal{N}^{y|x}$ is a completely positive map, there must exist (not uniquely) finitely many matrices $\{F_k^{y|x} \in \mathbb{C}^{\mathcal{S} \times \mathcal{S}}\}_k$ such that

$$[\mathcal{N}^{y|x}(\rho_S)] \equiv \sum_k F_k^{y|x} \cdot [\rho_S] \cdot (F_k^{y|x})^H \quad \forall \rho_S \in \mathfrak{D}(\mathcal{H}_S), \quad (46)$$

where $[\mathcal{N}^{y|x}(\rho_S)]$ and $[\rho_S]$ are respectively the matrix representation of the operator $\mathcal{N}^{y|x}(\rho_S)$ and ρ_S under $\{|s\rangle\}_{s \in \mathcal{S}}$. The reason for such matrices $\{F_k^{y|x}\}_k$ to exist is similar to that of the Kraus operators of CPTP maps (see Theorems 8.1 and 8.3 in [5]). Also note that $\sum_{y \in \mathcal{Y}} \mathcal{E}^{y|x}$ is trace preserving, thus it must hold that

$$\sum_{y \in \mathcal{Y}} \sum_k (F_k^{y|x})^H F_k^{y|x} = I \quad \forall x \in \mathcal{X}. \quad (47)$$

Now, define a set of functions $\{W^{y|x}\}_{x \in \mathcal{X}, y \in \mathcal{Y}}$ as

$$W^{y|x} : (s', s, \tilde{s}', \tilde{s}) \mapsto \sum_k F_k^{y|x}(s', s) \overline{F_k^{y|x}(\tilde{s}', \tilde{s})}, \quad (48)$$

for each $s', s, \tilde{s}', \tilde{s} \in \mathcal{S}$. One can rewrite (43), (44) and (45), respectively, into

$$P_{Y|X;S}(y|x; \rho_S) = \sum_{\substack{s', \tilde{s}' \\ s' = \tilde{s}'}} \sum_{s, \tilde{s}} W^{y|x}(s', s, \tilde{s}', \tilde{s}) \cdot [\rho_S]_{s, \tilde{s}}, \quad (49)$$

$$[\rho_{S'}]_{s', \tilde{s}'} = \frac{\sum_{s, \tilde{s}} W^{y|x}(s', s, \tilde{s}', \tilde{s}) \cdot [\rho_S]_{s, \tilde{s}}}{\sum_{s', \tilde{s}': s' = \tilde{s}'} \sum_{s, \tilde{s}} W^{y|x}(s', s, \tilde{s}', \tilde{s}) \cdot [\rho_S]_{s, \tilde{s}}}, \quad (50)$$

$$P_{Y_1^n | X_1^n; S_0}(\mathbf{y}_1^n | \mathbf{x}_1^n; \rho_{S_0}) = \sum_{s_n, \tilde{s}_n : s_n = \tilde{s}_n} \sum_{s_0^{n-1}, \tilde{s}_0^{n-1}} [\rho_{S_0}]_{s_0, \tilde{s}_0} \cdot \prod_{\ell=1}^n W^{y_\ell | x_\ell}(s_\ell, s_{\ell-1}, \tilde{s}_\ell, \tilde{s}_{\ell-1}). \quad (51)$$

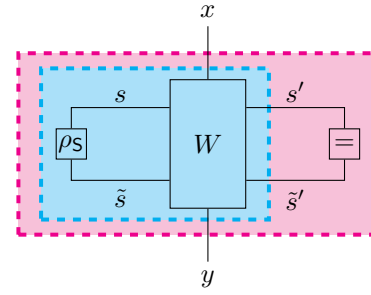


Fig. 5: Representation of $\{W^{y|x}\}_{x,y}$ using an NFG.

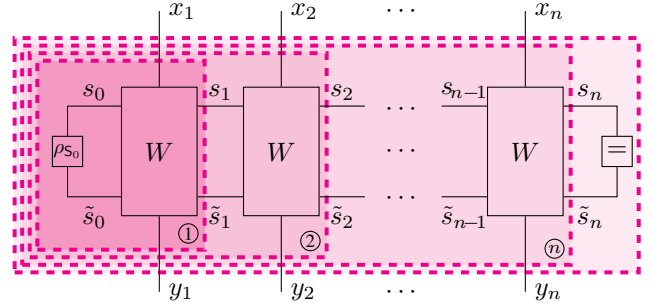


Fig. 6: The joint channel law (51) and (55) can be visualized as the result of the “closing of the outer most box” above, which can in turn be carried out by a sequence of “closing-the-box” operations as labeled.

By rearranging the entries of $W^{y|x}$ (for each x, y) into a matrix $[W^{y|x}] \in \mathbb{C}^{\mathcal{S}^2 \times \mathcal{S}^2}$ as

$$[W^{y|x}]_{(s', \tilde{s}'), (s, \tilde{s})} \triangleq W^{y|x}(s', s, \tilde{s}', \tilde{s}), \quad (52)$$

where $(s', \tilde{s}') \in \mathcal{S}^2$ is the first index, and $(s, \tilde{s}) \in \mathcal{S}^2$ is the second index of $[W^{y|x}]$, we can simplify (49), (50), and (51) as

$$P_{Y|X;S}(y|x; \rho_S) = \text{tr}([W^{y|x}] \cdot [\rho_S]), \quad (53)$$

$$[\rho_{S'}] = \frac{[W^{y|x}] \cdot [\rho_S]}{\text{tr}([W^{y|x}] \cdot [\rho_S])}, \quad (54)$$

$$P_{Y_1^n | X_1^n; S_0}(\mathbf{y}_1^n | \mathbf{x}_1^n; \rho_{S_0}) = \text{tr}([W^{y_n | x_n}] \cdots [W^{y_1 | x_1}] \cdot [\rho_{S_0}]), \quad (55)$$

respectively. Here we treat $[\rho_S]$ as a d^2 -length vector indexed by $(s, \tilde{s}) \in \mathcal{S}^2$ in the above equations.

By considering $\{W^{y|x}\}_{x,y}$ as a function of six variables, we can represent it using a factor node of degree six in an NFG as in Fig. 5. In this case, Eqs. (49) and (53) can be visualized as “closing the magenta box” in the NFG, i.e., summing over all the variables represented by the edges interior to the box. Similarly, (50) and (54) can be visualized as “closing the cyan box”. The NFG corresponding to using the channel n times consecutively is depicted in Fig. 6, where (51) and (55) are visualized as closing the outer most magenta box. Interestingly, this closing-the-box operation can be carried out by a sequence of simpler closing-the-box operations as shown in the figure.

A number of statistical quantities and density operators of interest can be computed as closing-the-box operations on

suitable NFGs similar to that of Fig. 6. The following example highlights how quantities of this kind can be computed in such a manner.

Example 5 (BCJR decoding for CC-QSCs). For fixed $\tilde{\mathbf{y}}_1^n \in \mathcal{Y}^n$ and a given initial density operator ρ_{S_0} , the conditional probability $P_{X_\ell | \mathcal{Y}_1^n; S_0}(x_\ell | \tilde{\mathbf{y}}_1^n; \rho_{S_0})$ can be computed via

$$P_{X_\ell | \mathcal{Y}_1^n; S_0}(\cdot | \tilde{\mathbf{y}}_1^n; \rho_{S_0}) \propto P_{X_\ell, \mathcal{Y}_1^n | S_0}(\cdot, \tilde{\mathbf{y}}_1^n | \rho_{S_0}), \quad (56)$$

where the RHS of (56) is a marginal pmf defined as

$$P_{X_\ell, \mathcal{Y}_1^n | S_0}(x_\ell, \tilde{\mathbf{y}}_1^n | \rho_{S_0}) = \sum_{\{x_k: k \neq \ell\}} \sum_{\mathbf{s}_0^n, \tilde{\mathbf{s}}_0^n} [\rho_{S_0}]_{s_0, \tilde{s}_0} \cdot \prod_{i=1}^n Q(x_i) \cdot \prod_{j=1}^n W^{\tilde{y}_j | x_j}(s_j, s_{j-1}, \tilde{s}_j, \tilde{s}_{j-1}), \quad (57)$$

where we have assumed that the input process X_1^n is i.i.d. characterized by some pmf Q . The evaluation of (57) can be carried out efficiently using a sequence of closing-the-box operations as visualized in Fig. 7. These operations can be roughly divided into the following three steps.

- 1) Closing the magenta box: this results in an operator $\frac{\sigma_{S_{\ell-1}}^{\tilde{\mathbf{y}}_1^{\ell-1}}}{\sigma_{S_{\ell-1}}}$ on $\mathcal{H}_{S_{\ell-1}}$.
- 2) Closing the cyan box: this results in another operator $\frac{\sigma_{S_\ell}^{\tilde{\mathbf{y}}_1^\ell}}{\sigma_{S_\ell}}$ on \mathcal{H}_{S_ℓ} .
- 3) Applying the closing-the-box operation to the yellow box: the result is the marginal pmf $P_{X_\ell, \mathcal{Y}_1^n | S_0}(x_\ell, \tilde{\mathbf{y}}_1^n | \rho_{S_0})$, from which the desired conditional probability $P_{X_\ell | \mathcal{Y}_1^n; S_0}(x_\ell | \tilde{\mathbf{y}}_1^n; \rho_{S_0})$ can be easily obtained by normalization.

The operators mentioned in 1) and 2) can be computed recursively, using a sequence of closing-the-box operations. Namely, one can carry out the computations in 1) consecutively with $\ell = 1, 2, \dots, n$; or the computations in 2) consecutively with $\ell = n, n-1, \dots, 1$. This provides an efficient way to evaluate $P_{X_\ell | \mathcal{Y}_1^n; S_0}(x_\ell | \tilde{\mathbf{y}}_1^n; \rho_{S_0})$ for each $\ell = 1, \dots, n$; and thus provides an efficient symbol-wise decoding algorithm. The idea in this example is identical to that of the BCJR decoding algorithm for an FSMC. \square

As shown in the above example, very often the desired functions or quantities are based on the same partial results. The NFG framework is very helpful to visualize these partial results and to show how they can be combined to obtain the desired functions and quantities.

We emphasize that the functions $\{W^{y|x}\}_{x,y}$ defined in (48) are unique for a given finite-dimensional CC-QSC $\{\mathcal{N}^{y|x}\}_{x,y}$; even though such uniqueness does not apply to the Kraus operators $\{F^{y|x}\}_k$ being used to define $\{W^{y|x}\}_{x,y}$. This can be proven by making the identification that

$$[\mathcal{N}^{y|x}(\rho_S)] \equiv [W^{y|x}] \cdot [\rho_S] \quad \forall \rho_S \in \mathcal{D}(\mathcal{H}_S), \quad (58)$$

for all x and y . Moreover, we argue that the functions $\{W^{y|x}\}_{x,y}$, are an *equivalent* way to specify a CC-QSC, or classical communication over a quantum channel with memory as described at the beginning of this section. Namely, for any set of convex-valued functions $\{W^{y|x}\}_{x,y}$ on \mathcal{S}^4 satisfying some constrains to be clarified later, there must

exist a unique CC-QSC $\{\mathcal{N}^{y|x}\}_{x,y}$ such that (58) holds; and thus, there must exist some corresponding channel-ensemble-measurement configuration, unique up to its channel law. As for such constrains, we rearrange the entries of $W^{y|x}$ (for each x, y) into another matrix $[[W^{y|x}]] \in \mathbb{C}^{\mathcal{S}^2 \times \mathcal{S}^2}$, whose entries are defined as

$$[[W^{y|x}]]_{(s',s),(\tilde{s}',\tilde{s})} \triangleq W^{y|x}(s',s,\tilde{s}',\tilde{s}), \quad (59)$$

where $(s',s) \in \mathcal{S}^2$ is the first index, and $(\tilde{s}',\tilde{s}) \in \mathcal{S}^2$ is the second index of $[[W^{y|x}]]$. Notice that, $[[W^{y|x}]]$ is a positive semi-definite (p.s.d.) matrix, and it satisfies the following equation

$$\sum_{y \in \mathcal{Y}} \sum_{s', \tilde{s}': s' = \tilde{s}'} [[W^{y|x}]]_{(s',s),(\tilde{s}',\tilde{s})} = \delta_{s,\tilde{s}} \quad \forall x \in \mathcal{X}, \quad (60)$$

where $\delta_{s,\tilde{s}}$ is the Kronecker-delta function. In this case, the “equivalence” can be shown by the following proposition.

Proposition 6. *Let \mathcal{X}, \mathcal{Y} be finite sets, and \mathcal{H}_S be a finite-dimensional Hilbert space with an orthonormal basis $\{|s\rangle\}_{s \in \mathcal{S}}$. For any class of functions*

$$\{W^{y|x} : \mathcal{S} \times \mathcal{S} \times \mathcal{S} \times \mathcal{S} \rightarrow \mathbb{C}\}_{x \in \mathcal{X}, y \in \mathcal{Y}}$$

such that its matrix form $\{[[W^{y|x}]]\}_{x,y}$ consists of p.s.d. matrices and satisfies (60), there must exist a unique unique CC-QSC $\{\mathcal{N}^{y|x}\}_{x,y}$ acting on \mathcal{H}_S such that (58) holds.

Proof. The idea of the proof is to consider the eigenvalue decomposition of $[[W^{y|x}]]$, and reconstruct $\mathcal{N}^{y|x}$ by following the equations (48) and (46) backwardly. This process is straightforward, and we omit the details here. \square

Let us conclude this section by pointing out that the functions $\{W^{y|x}\}_{x,y}$, particularly the corresponding NFG, can be constructed from the channel-ensemble-measurement configuration $(\mathcal{N}, \{\rho_A^{(x)}\}_{x \in \mathcal{X}}, \{\Lambda_B^{(y)}\}_{y \in \mathcal{Y}})$ as in Fig. 8. This can be justified by checking (42) and (58).

IV. INFORMATION RATE AND ITS ESTIMATION

In this section, we focus on the information rate of the communication scheme described in Section III. As defined in (1), the information rate is the limit superior of the average mutual information $\frac{1}{n} \mathbf{I}(X_1^n; Y_1^n)$ between the input and output processes X_1^n and Y_1^n as n tends to infinity. We assume that X_1^n is distributed according to some i.i.d. process³ characterized by the pmf Q , i.e., $Q^{(n)}(\mathbf{x}_1^n) = \prod_{\ell=1}^n Q(x_\ell)$. In this case, the joint distribution of (X_1^n, Y_1^n) is given by

$$P_{X_1^n, Y_1^n | S_0}(\mathbf{x}_1^n, \mathbf{y}_1^n | \rho_{S_0}) = \left(\prod_{\ell=1}^n Q(x_\ell) \right) \cdot P_{Y_1^n | X_1^n, S_0}(\mathbf{y}_1^n | \mathbf{x}_1^n; \rho_{S_0}), \quad (61)$$

where $P_{Y_1^n | X_1^n, S_0}$ is specified in (40), (45), (51) or (55), depending on which notation we use to specify the channel (see Proposition 4 and 6). It is obvious that the value of (61), and thus the information rate, depends on the initial density operator ρ_{S_0} . In this sense, we denote the information rate

³For more general type of sources, like a finite-state-machine source (FSMS), one can consider “merging” the memory of the source into that of the channel, and thus obtaining an equivalent memoryless input process.

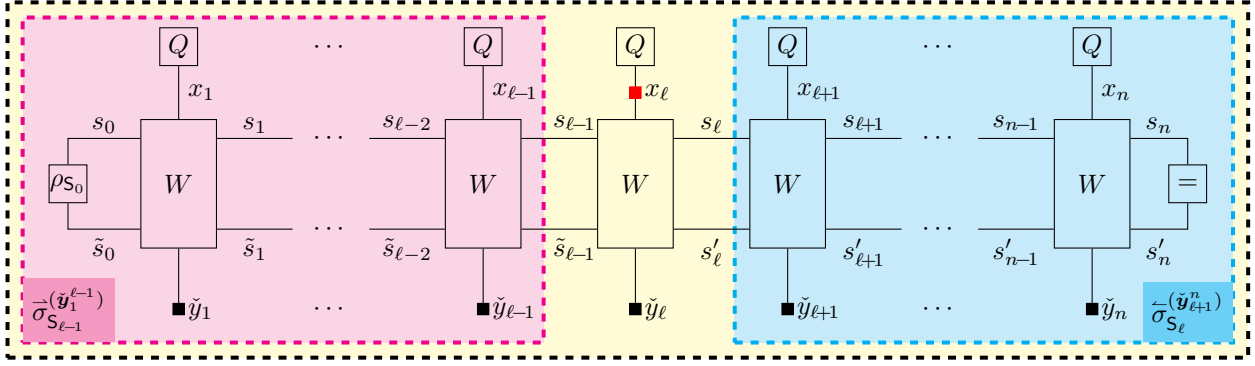


Fig. 7: Computation of the marginal pmf $P_{X_\ell | Y_1^n; S_0}$ using a sequence of closing-the-box operations.

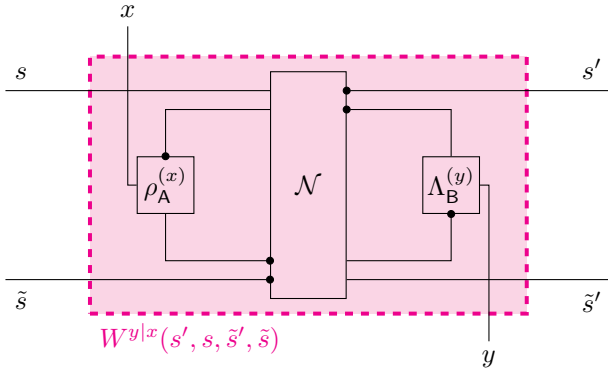


Fig. 8: NFG representation of the channel-ensemble-measurement configuration $(\mathcal{N}, \{\rho_A^{(x)}\}_{x \in \mathcal{X}}, \{\Lambda_B^{(y)}\}_{y \in \mathcal{Y}})$.

as a function of the input pmf Q , the CC-QSC $\{\mathcal{N}^{y|x}\}_{x,y}$ describing the communication, and the initial density operator ρ_{S_0} , namely

$$I(Q, \{\mathcal{N}^{y|x}\}_{x,y}, \rho_{S_0}) \triangleq \limsup_{n \rightarrow \infty} I^{(n)}(Q, \{\mathcal{N}^{y|x}\}_{x,y}, \rho_{S_0}), \quad (62)$$

$$I^{(n)}(Q, \{\mathcal{N}^{y|x}\}_{x,y}, \rho_{S_0}) \triangleq \frac{1}{n} \mathbf{I}(X_1^n; Y_1^n)(\rho_{S_0}). \quad (63)$$

Here, $\mathbf{I}(X_1^n; Y_1^n)(\rho_{S_0})$ is the mutual information between X_1^n and Y_1^n ; and the latter are jointly distributed according to (61). The argument ρ_{S_0} emphasizes the dependency of $\frac{1}{n} \mathbf{I}(X_1^n; Y_1^n)$ on ρ_{S_0} .

Similar to the case of an FSMC, the dependency of the information rate on the initial density operator usually cannot be ignored. However, as already mentioned in Section II-B, for a class of FSMCs, namely the indecomposable FSMCs, it is known that the information rate is independent from the initial channel state [11]. An indecomposable FSMC, intuitively speaking, is an FSMC whose state distribution, given different initial states, tends to be indistinguishable as $n \rightarrow \infty$, independently of the input sequence realized. A quantum analogy was proposed by Bowen, Devetak, and Mancini [31], where they defined the indecomposable quantum channels with memory, and proved that the quantum entropic bound for such channels is independent from the initial density operator.

In the remainder of this section we firstly define the indecomposability of CC-QSCs, and prove the independence of the

information rate as in (62) from the initial density operator. Secondly, we generalize the method as in Algorithm 2 in estimating such information rates efficiently.

The definition of an indecomposable CC-QSC in our paper is similar (but different) and closely related to that of an indecomposable (quantum) memory channel in [31]. Namely, an indecomposable memory channel equipped with separable input ensemble and local output measurement will always induce an indecomposable CC-QSC, but not necessarily vice versa. Moreover, in [31] the classical capacity of quantum channels with finite memory was considered, where the capacity is essentially the Holevo bound, and where the latter was proven to be achievable [2]. However, in our work, we focus on the situation where the ensemble and the measurement are fixed.

A. Indecomposable Quantum-State Channel

Definition 7. A CC-QSC $\{\mathcal{N}^{y|x}\}_{x,y}$ is said to be *indecomposable* if for any initial density operators α_{S_0} and β_{S_0} , the following statement holds: for any $\epsilon > 0$, there always exists some positive integer N s.t.

$$\left\| \alpha_{S_n}^{(x_1^n)} - \beta_{S_n}^{(x_1^n)} \right\| < \epsilon \quad \forall n \geq N, \quad \forall x_1^n, \quad (64)$$

where

$$\alpha_{S_n}^{(x_1^n)} \triangleq \sum_{y_1^n} \mathcal{N}^{y_n|x_n} \circ \dots \circ \mathcal{N}^{y_1|x_1}(\alpha_{S_0}), \quad (65)$$

$$\beta_{S_n}^{(x_1^n)} \triangleq \sum_{y_1^n} \mathcal{N}^{y_n|x_n} \circ \dots \circ \mathcal{N}^{y_1|x_1}(\beta_{S_0}), \quad (66)$$

and where $\|A\|$ is the trace distance for an operator A on \mathcal{H}_S , i.e., $\|A\| \triangleq \frac{1}{2} \text{tr} \sqrt{A^\dagger A}$. \square

Theorem 8. *The information rate of an indecomposable CC-QSC with an i.i.d. input process is independent of the initial density operator. Namely, if $\{\mathcal{N}^{y|x}\}_{x,y}$ is indecomposable, then*

$$I^{(n)}(Q, \{\mathcal{N}^{y|x}\}_{x,y}, \alpha_{S_0}) - I^{(n)}(Q, \{\mathcal{N}^{y|x}\}_{x,y}, \beta_{S_0}) \xrightarrow{n \rightarrow \infty} 0, \quad \text{for any initial density operators } \alpha_{S_0}, \beta_{S_0} \in \mathcal{D}(\mathcal{H}_{S_0}).$$

In the proof below, we follow a similar idea as in [11] for indecomposable FSMCs, and as that in [31] for indecomposable quantum channel with memory. The proof uses Lemma 9 as

shown and proven below, followed by the proof of the theorem.

Lemma 9. *Let A, B, C be quantum systems described by some finite-dimensional Hilbert spaces \mathcal{H}_A , \mathcal{H}_B , \mathcal{H}_C , respectively. Suppose the joint density operator ρ_{ABC} satisfies*

$$\rho_{AB} = (I_A \otimes \Phi)(\rho_{AC}),$$

for some CPTP map $\Phi : \mathfrak{D}(\mathcal{H}_C) \rightarrow \mathfrak{D}(\mathcal{H}_B)$. Then, the following inequalities must hold

$$0 \leq \mathbf{I}(A; B) \leq \mathbf{I}(A; C). \quad (67)$$

Proof. The first inequality in (67) is a direct result of the subadditivity inequality for the von Neumann entropy.

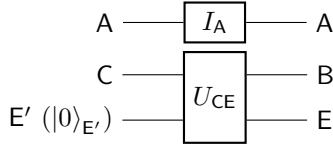
The second inequality in (67) can be proven as follows. Namely, since Φ is CPTP, there must exist some environment system E, and some unitary operator U_{CE} on the joint system CE such that

$$\Phi(\rho_C) \equiv \text{tr}_E (U_{CE}(\rho_C \otimes |0_E\rangle\langle 0_E|)U_{CE}^H) \quad \forall \rho_C \in \mathfrak{D}(\mathcal{H}_C).$$

In this case, $\rho_{AB} = \text{tr}_E \rho_{ABE}$, where

$$\rho_{ABE} \triangleq (I_A \otimes U_{CE}) \cdot (\rho_{AC} \otimes |0_E\rangle\langle 0_E|) \cdot (I_A \otimes U_{CE}^H).$$

The above equality can be illustrated as follows, where we use E' to denote the system E before the operation U_{CE} :



The second inequality of (67) follows from

$$\mathbf{I}(A; C) \stackrel{(a)}{=} \mathbf{I}(A; CE') \stackrel{(b)}{=} \mathbf{I}(A; BE) \stackrel{(c)}{\geq} \mathbf{I}(A; B),$$

where (a) is due to the fact that E' is in a pure state, (b) is true because applying the unitary operation $I_A \otimes U_{CE}$ does not affect the mutual information, and (c) is can be derived using the monotonicity of von Neumann mutual information. \square

Proof of Theorem 8. Let A and B be quantum systems described by Hilbert spaces \mathcal{H}_A and \mathcal{H}_B , respectively, where $\{|x\rangle\}_{x \in \mathcal{X}}$ and $\{|y\rangle\}_{y \in \mathcal{Y}}$ are orthonormal bases of \mathcal{H}_A and \mathcal{H}_B , respectively. Let A_1^n and B_1^n be n independent copies of A and B, respectively. Let ρ_{S_0} be some initial density operator; and let the joint density operator on system $A_1^n B_1^n$ be

$$\rho_{A_1^n B_1^n} \triangleq \sum_{\mathbf{x}_1^n} Q(\mathbf{x}_1^n) \cdot |\mathbf{x}_1^n\rangle\langle \mathbf{x}_1^n| \otimes \sum_{\mathbf{y}_1^n} \text{tr} \left(\mathcal{N}^{\mathbf{y}_1^n | \mathbf{x}_1^n}(\rho_{S_0}) \right) \cdot |\mathbf{y}_1^n\rangle\langle \mathbf{y}_1^n|,$$

where $\mathcal{N}^{\mathbf{y}_1^n | \mathbf{x}_1^n} \triangleq \mathcal{N}^{y_n | x_n} \circ \dots \circ \mathcal{N}^{y_1 | x_1}$. In this case, it is not hard to see that

$$\mathbf{I}(X_1^n; Y_1^n) [\rho_{S_0}] = \mathbf{I}(A_1^n; B_1^n) [\rho_{S_0}].$$

In fact, one can easily check that

$$\begin{aligned} \mathbf{H}(A_1^n) &= \mathbf{H}(X_1^n), \\ \mathbf{H}(B_1^n) &= \mathbf{H}(Y_1^n), \\ \mathbf{H}(A_1^n, B_1^n) &= \mathbf{H}(X_1^n, Y_1^n). \end{aligned}$$

Particularly, $\mathbf{H}(A_1^n)$ is independent from the initial density operator ρ_{S_0} . We also claim that, for each $\rho_{S_0} \in \mathfrak{D}(\mathcal{H}_{S_0})$,

$$\mathbf{I}(A_1^N B_1^N; A_{N+1}^n B_{N+1}^n) \leq 2\mathbf{H}(S_N), \quad (68)$$

$$\mathbf{I}(B_1^N; B_{N+1}^n) \leq 2\mathbf{H}(S_N), \quad (69)$$

where the density operator for S_N is defined according to ρ_{S_0} as

$$\rho_{S_N} \triangleq \sum_{\mathbf{x}_1^N} Q(\mathbf{x}_1^N) \cdot \sum_{\mathbf{y}_1^N} \mathcal{N}^{\mathbf{y}_1^N | \mathbf{x}_1^N}(\rho_{S_0}).$$

Proof of (68): We define a class of CPTP maps $\{\Phi_a^b : \mathfrak{D}(\mathcal{H}_{S_a}) \rightarrow \mathfrak{D}(\mathcal{H}_{A_a^b B_a^b})\}_{b>a \in \mathbb{N}}$ as

$$\Phi_a^b : \rho_{S_a} \mapsto \sum_{\mathbf{x}_a^b} Q(\mathbf{x}_a^b) \cdot |\mathbf{x}_a^b\rangle\langle \mathbf{x}_a^b| \otimes \sum_{\mathbf{y}_a^b} \text{tr} \left(\mathcal{N}^{\mathbf{y}_a^b | \mathbf{x}_a^b}(\rho_{S_a}) \right) \cdot |\mathbf{y}_a^b\rangle\langle \mathbf{y}_a^b|.$$

Since the input process Q is i.i.d., we can rewrite $\rho_{A_1^n B_1^n}$, for each positive integer $N < n$, as

$$\rho_{A_1^n B_1^n} = \left(I_{A_1^N B_1^N} \otimes \Phi_{N+1}^n \right) \left(\rho_{A_1^N B_1^N} \rho_{S_N} \right),$$

where

$$\rho_{A_1^N B_1^N} \rho_{S_N} \triangleq \sum_{\mathbf{x}_1^N} Q(\mathbf{x}_1^N) \cdot |\mathbf{x}_1^N\rangle\langle \mathbf{x}_1^N| \otimes \sum_{\mathbf{y}_1^N} \mathcal{N}^{\mathbf{y}_1^N | \mathbf{x}_1^N}(\rho_{S_0}) \cdot |\mathbf{y}_1^N\rangle\langle \mathbf{y}_1^N|.$$

Hence, by Lemma 9, one must have

$$\mathbf{I}(A_1^N B_1^N; A_{N+1}^n B_{N+1}^n) \leq \mathbf{I}(A_1^N B_1^N; S_N).$$

Additionally, by subadditivity of joint entropy, we have

$$\begin{aligned} \mathbf{I}(A_1^N B_1^N; S_N) &\triangleq \mathbf{H}(A_1^N B_1^N) + \mathbf{H}(S_N) - \mathbf{H}(A_1^N B_1^N S_N) \\ &\leq \mathbf{H}(A_1^N B_1^N) + \mathbf{H}(S_N) - |\mathbf{H}(A_1^N B_1^N) - \mathbf{H}(S_N)| \\ &\leq 2\mathbf{H}(S_N). \end{aligned}$$

Combining the above two inequalities, we have proven (68).

Proof of (69): We follow the same approach as above by defining a class of CPTP maps $\{\Psi_a^b : \}_{b>a \in \mathbb{N}}$ as

$$\Psi_a^b : \rho_{S_a} \mapsto \sum_{\mathbf{x}_a^b} Q(\mathbf{x}_a^b) \cdot \sum_{\mathbf{y}_a^b} \text{tr} \left(\mathcal{N}^{\mathbf{y}_a^b | \mathbf{x}_a^b}(\rho_{S_a}) \right) \cdot |\mathbf{y}_a^b\rangle\langle \mathbf{y}_a^b|.$$

We omit the detailed derivation of 69 here.

We now return to the main proof. Given the initial density operators α_{S_0} , and β_{S_0} , we define $\alpha_{A_1^n B_1^n}$, $\beta_{A_1^n B_1^n}$ and α_{S_N} , β_{S_N} in a similar fashion as we have defined $\rho_{A_1^n B_1^n}$ and ρ_{S_N} based on ρ_{S_0} . In this case, one can show that

$$\begin{aligned} & \left| \mathbf{H}(\alpha_{A_1^n B_1^n}) - \mathbf{H}(\beta_{A_1^n B_1^n}) \right| - \left| \mathbf{H}(\alpha_{A_{N+1}^n B_{N+1}^n}) - \mathbf{H}(\beta_{A_{N+1}^n B_{N+1}^n}) \right| \\ & \stackrel{(a)}{\leq} \left| \mathbf{H}(\alpha_{A_1^N B_1^N}) - \mathbf{H}(\beta_{A_1^N B_1^N}) \right| + \left| \mathbf{I}(A_1^N B_1^N; A_{N+1}^n B_{N+1}^n) [\alpha_{A_1^n B_1^n}] \right. \\ & \quad \left. - \mathbf{I}(A_1^N B_1^N; A_{N+1}^n B_{N+1}^n) [\beta_{A_1^n B_1^n}] \right| \\ & \stackrel{(b)}{\leq} N \cdot \log(\dim \mathcal{H}_{AB}) + 2 \cdot \left| \mathbf{H}(\alpha_{S_N}) - \mathbf{H}(\beta_{S_N}) \right|, \quad (70) \end{aligned}$$

where we have used the triangle inequality (twice) in step (a), and (68) in step (b). Similarly, using (69), one can prove

$$\begin{aligned} & \left| \mathbf{H}(\alpha_{B_1^n}) - \mathbf{H}(\beta_{B_1^n}) \right| - \left| \mathbf{H}(\alpha_{B_{N+1}^n}) - \mathbf{H}(\beta_{B_{N+1}^n}) \right| \\ & \leq N \cdot \log(\dim \mathcal{H}_B) + 2 \cdot \left| \mathbf{H}(\alpha_{S_N}) - \mathbf{H}(\beta_{S_N}) \right|. \quad (71) \end{aligned}$$

Assuming $\max\{\dim \mathcal{H}_A, \dim \mathcal{H}_B, \dim \mathcal{H}_S\} \leq d$ for some integer d , we have

$$\begin{aligned}
& \frac{1}{n} |\mathbf{I}(X_1^n; Y_1^n)[\alpha_{S_0}] - \mathbf{I}(X_1^n; Y_1^n)[\beta_{S_0}]| \\
&= \frac{1}{n} |\mathbf{I}(A_1^n; B_1^n)[\alpha_{S_0}] - \mathbf{I}(A_1^n; B_1^n)[\beta_{S_0}]| \\
&= \frac{1}{n} |(\mathbf{H}(\alpha_{B_1^n}) - \mathbf{H}(\alpha_{A_1^n B_1^n})) - (\mathbf{H}(\beta_{B_1^n}) - \mathbf{H}(\beta_{A_1^n B_1^n}))| \\
&\stackrel{(c)}{\leq} \frac{1}{n} |\mathbf{H}(\alpha_{B_1^n}) - \mathbf{H}(\beta_{B_1^n})| + \frac{1}{n} |\mathbf{H}(\alpha_{A_1^n B_1^n}) - \mathbf{H}(\beta_{A_1^n B_1^n})| \\
&\stackrel{(d)}{\leq} \frac{3N+4}{n} \cdot \log d + \frac{1}{n} |\mathbf{H}(\alpha_{B_{N+1}^n}) - \mathbf{H}(\beta_{B_{N+1}^n})| \\
&\quad + \frac{1}{n} |\mathbf{H}(\alpha_{A_{N+1}^n B_{N+1}^n}) - \mathbf{H}(\beta_{A_{N+1}^n B_{N+1}^n})| \\
&= \frac{3N+4}{n} \cdot \log d + \frac{1}{n} |\mathbf{H}(\Phi_{N+1}^n(\alpha_{S_N})) - \mathbf{H}(\Phi_{N+1}^n(\beta_{S_N}))| \\
&\quad + \frac{1}{n} |\mathbf{H}(\Psi_{N+1}^n(\alpha_{S_N})) - \mathbf{H}(\Psi_{N+1}^n(\beta_{S_N}))|
\end{aligned}$$

where we have used the triangle inequality in step (c), and (70), (71) in step (d). Using Fannes' inequality, we have

$$\begin{aligned}
& \frac{1}{n} |\mathbf{H}(\Phi_{N+1}^n(\alpha_{S_N})) - \mathbf{H}(\Phi_{N+1}^n(\beta_{S_N}))| \\
&\leq \frac{\log d^{n-N}}{n} \left(\|\Phi_{N+1}^n(\alpha_{S_N}) - \Phi_{N+1}^n(\beta_{S_N})\| \right. \\
&\quad \left. + \eta(\|\Phi_{N+1}^n(\alpha_{S_N}) - \Phi_{N+1}^n(\beta_{S_N})\|) \right) \\
& \frac{1}{n} |\mathbf{H}(\Psi_{N+1}^n(\alpha_{S_N})) - \mathbf{H}(\Psi_{N+1}^n(\beta_{S_N}))| \\
&\leq \frac{\log d^{2(n-N)}}{n} \left(\|\Psi_{N+1}^n(\alpha_{S_N}) - \Psi_{N+1}^n(\beta_{S_N})\| \right. \\
&\quad \left. + \eta(\|\Psi_{N+1}^n(\alpha_{S_N}) - \Psi_{N+1}^n(\beta_{S_N})\|) \right)
\end{aligned}$$

where

$$\eta(x) \triangleq \begin{cases} -x \log x & 0 \leq x < e^{-1}, \\ e^{-1} & x \geq e^{-1}. \end{cases}$$

Moreover, by the contractivity of trace distance, we have,

$$\begin{aligned}
\|\Phi_{N+1}^n(\alpha_{S_N}) - \Phi_{N+1}^n(\beta_{S_N})\| &\leq \|\alpha_{S_N} - \beta_{S_N}\|, \\
\|\Psi_{N+1}^n(\alpha_{S_N}) - \Psi_{N+1}^n(\beta_{S_N})\| &\leq \|\alpha_{S_N} - \beta_{S_N}\|.
\end{aligned}$$

Also noticing that η is monotonically increasing, and $\eta(x) < x$ for all $x > 0$, we can write

$$\begin{aligned}
& \frac{1}{n} |\mathbf{I}(X_1^n; Y_1^n)[\alpha_{S_0}] - \mathbf{I}(X_1^n; Y_1^n)[\beta_{S_0}]| \\
&\leq \left(\frac{3N+4}{n} + \frac{6(n-N)}{n} \cdot \|\alpha_{S_n} - \beta_{S_n}\| \right) \cdot \log d.
\end{aligned}$$

Finally, because the CC-QSC is indecomposable, for any $\varepsilon > 0$, we can choose N large enough such that

$$\|\alpha_{S_N} - \beta_{S_N}\| < \frac{\varepsilon}{12 \cdot \log d},$$

and choose an integer $M > N$ such that

$$\frac{3N+4}{M} \cdot \log d < \frac{\varepsilon}{2}.$$

This will ensure that for any $n > M$, we have

$$\left(\frac{3N+4}{n} + \frac{6(n-N)}{n} \cdot \|\alpha_{S_n} - \beta_{S_n}\| \right) \cdot \log d < \varepsilon,$$

which concludes the proof of the theorem. \square

B. Estimation of the Information Rate

The development in this section is very similar to the development in Section II-B. In particular, we follow the same logic as in Eqs. (10)–(17). This similarity stems from the similarity of the NFGs in Figs. 4 and 7, and highlights one of the benefits of the factor-graph approach that we take to estimate information rates of quantum channels with memory.

We make the following assumptions.

- As already mentioned, the derivations in this paper are for the case where the input process $X_1^n = (X_1, \dots, X_n)$ is an i.i.d. process. The results can be generalized to other stationary ergodic input processes that can be represented by a finite-state-machine source (FSMS). Technically, this is done by defining a new state that combines the FSMS state and the channel state.
- We assume that the corresponding quantum-state channel $\{\mathcal{N}^{y|x}\}_{x \in \mathcal{X}, y \in \mathcal{Y}}$ is finite-dimensional and indecomposable. We also assume it can be represented by some functions $\{W^{y|x}\}_{x,y}$ as defined in (48).

The major difference compared with Section II-B is the conditional pmf $P_{Y_1^n | X_1^n, S_0}$, and thus the joint pmf $P_{Y_1^n, X_1^n | S_0}$ as specified in (55) and (61), respectively. In this case, in order to compute $-\frac{1}{n} \log P_{Y_1^n}(\tilde{y}_1^n)$ and $-\frac{1}{n} \log P_{X_1^n, Y_1^n}(\tilde{x}_1^n, \tilde{y}_1^n)$ using a similar method as in Section II-B, we consider state metrics $\{\sigma_\ell^Y\}_{\ell=1}^n$ and $\{\sigma_\ell^{XY}\}_{\ell=1}^n$ (which are operators on \mathcal{H}_{S_ℓ} for each ℓ) defined w.r.t. \tilde{y}_1^n and w.r.t. \tilde{x}_1^n and \tilde{y}_1^n , respectively, as

$$\sigma_\ell^Y \triangleq \sum_{\mathbf{x}_\ell^1} Q^{(\ell)}(\mathbf{x}_\ell^1) \cdot \mathcal{N}^{\tilde{y}_n | x_n} \circ \dots \circ \mathcal{N}^{\tilde{y}_1 | x_1}(\rho_{S_0}), \quad (72)$$

$$\sigma_\ell^{XY} \triangleq \mathcal{N}^{\tilde{y}_n | \tilde{x}_n} \circ \dots \circ \mathcal{N}^{\tilde{y}_1 | \tilde{x}_1}(\rho_{S_0}). \quad (73)$$

One can verify that

$$P_{Y_1^n}(\tilde{y}_1^n) = \text{tr}(\sigma_\ell^Y), \quad (74)$$

$$P_{X_1^n, Y_1^n}(\tilde{x}_1^n, \tilde{y}_1^n) = \text{tr}(\sigma_\ell^{XY}), \quad (75)$$

where $\{\sigma_\ell^Y\}_\ell$ and $\{\sigma_\ell^{XY}\}_\ell$ can be computed iteratively as

$$[\sigma_\ell^Y] = \sum_{x_\ell} Q(x_\ell) \cdot [W^{y|x}] \cdot [\sigma_{\ell-1}^Y], \quad (76)$$

$$[\sigma_\ell^{XY}] = [W^{y|x}] \cdot [\sigma_{\ell-1}^Y], \quad (77)$$

where we treat $[\sigma_\ell^Y]$ and $[\sigma_\ell^{XY}]$ as a length- d^2 vector indexed by $(s, \bar{s}) \in S^2$ in the above two equations. (See (52) and (55) for notation.) Additionally, we can also introduce normalizing coefficients $\{\lambda_\ell^Y\}_\ell$ and $\{\lambda_\ell^{XY}\}_\ell$, similar to (22), in order to keep the trace of the operators to be equal to 1

The above discussion is summarized as Algorithm 10. The computations corresponding to Line 3, Lines 5–9 and Lines 12–16 are visualized in Figs. 17, 19, and 21 in the Appendix, respectively.

V. INFORMATION RATE UPPER/LOWER BOUNDS AND THEIR OPTIMIZATION

In this section, we consider auxiliary channels and their induced upper and lower bounds on the information rate. In particular, we consider the auxiliary channels chosen from the domain of all CC-QSCs with the same input and output alphabet as the original channel, and acting on a memory system of

$$\bar{\mathbb{I}}^{(n)}(\hat{W}) = \frac{1}{n} \left\langle \log \frac{\text{tr}([W^{Y_n|X_n}] \dots [W^{Y_1|X_1}] \cdot [\rho_{S_0}])}{\sum_{\mathbf{x}_1^n} Q^{(n)}(\mathbf{x}_1^n) \cdot \text{tr}([\hat{W}^{Y_n|x_n}] \dots [\hat{W}^{Y_1|x_1}] \cdot [\rho_{\hat{S}_0}])} \right\rangle \quad (78)$$

$$\underline{\mathbb{I}}^{(n)}(\hat{W}) = \frac{1}{n} \left\langle \log \frac{\text{tr}([\hat{W}^{Y_n|X_n}] \dots [\hat{W}^{Y_1|X_1}] \cdot [\rho_{\hat{S}_0}])}{\sum_{\mathbf{x}_1^n} Q^{(n)}(\mathbf{x}_1^n) \cdot \text{tr}([\hat{W}^{Y_n|x_n}] \dots [\hat{W}^{Y_1|x_1}] \cdot [\rho_{\hat{S}_0}])} \right\rangle \quad (79)$$

$$\Delta^{(n)}(\hat{W}) = \frac{1}{n} \left\langle \log \frac{\text{tr}([W^{Y_n|X_n}] \dots [W^{Y_1|X_1}] \cdot [\rho_{S_0}])}{\text{tr}([\hat{W}^{Y_n|X_n}] \dots [\hat{W}^{Y_1|X_1}] \cdot [\rho_{\hat{S}_0}])} \right\rangle \quad (80)$$

$$\frac{d}{dt} \Big|_{t=0} \bar{\mathbb{I}}^{(n)}(\hat{W} + tH) \propto -\frac{1}{n} \left\langle \sum_{k=1}^n \sum_{\mathbf{x}_1^n} Q^{(n)}(\mathbf{x}_1^n) \cdot \text{tr}([\hat{W}^{Y_n|x_n}] \dots [\hat{W}^{Y_{k+1}|x_{k+1}}][H^{Y_k|x_k}][\hat{W}^{Y_{k-1}|x_{k-1}}] \dots [\hat{W}^{Y_1|x_1}] \cdot [\rho_{\hat{S}_0}]) \right\rangle \quad (81)$$

$$= -\frac{1}{n} \sum_{\mathbf{x}_1^n, \mathbf{y}_1^n} P_{X_1^n, Y_1^n | S_0}(\mathbf{x}_1^n, \mathbf{y}_1^n | \rho_{S_0}) \cdot \sum_k \sum_{s', s, \tilde{s}', \tilde{s}} \bar{\varrho}_{\hat{S}_{k-1}}^{(\mathbf{y}_1^{k-1})}(s, \tilde{s}) \cdot H^{y_k|x_k}(s', s, \tilde{s}', \tilde{s}) \cdot \bar{\varrho}_{\hat{S}_k}^{(\mathbf{y}_{k+1}^n)}(s', \tilde{s}') \quad (82)$$

$$\frac{d}{dt} \Big|_{t=0} \underline{\mathbb{I}}^{(n)}(\hat{W} + tH) \propto -\frac{1}{n} \left\langle \sum_{k=1}^n \sum_{\mathbf{x}_1^n} Q^{(n)}(\mathbf{x}_1^n) \cdot \text{tr}([\hat{W}^{Y_n|x_n}] \dots [\hat{W}^{Y_{k+1}|x_{k+1}}][H^{Y_k|x_k}][\hat{W}^{Y_{k-1}|x_{k-1}}] \dots [\hat{W}^{Y_1|x_1}] \cdot [\rho_{\hat{S}_0}]) \right\rangle \quad (83)$$

$$+ \frac{1}{n} \left\langle \sum_{k=1}^n \text{tr}([\hat{W}^{Y_n|X_n}] \dots [\hat{W}^{Y_{k+1}|X_{k+1}}][H^{Y_k|X_k}][\hat{W}^{Y_{k-1}|X_{k-1}}] \dots [\hat{W}^{Y_1|X_1}] \cdot [\rho_{\hat{S}_0}]) \right\rangle$$

$$= -\frac{1}{n} \sum_{\mathbf{x}_1^n, \mathbf{y}_1^n} P_{X_1^n, Y_1^n | S_0}(\mathbf{x}_1^n, \mathbf{y}_1^n | \rho_{S_0}) \cdot \sum_k \sum_{s', s, \tilde{s}', \tilde{s}} \bar{\varrho}_{\hat{S}_{k-1}}^{(\mathbf{y}_1^{k-1})}(s, \tilde{s}) \cdot H^{y_k|x_k}(s', s, \tilde{s}', \tilde{s}) \cdot \bar{\varrho}_{\hat{S}_k}^{(\mathbf{y}_{k+1}^n)}(s', \tilde{s}') \quad (84)$$

$$+ \frac{1}{n} \sum_{\mathbf{x}_1^n, \mathbf{y}_1^n} P_{X_1^n, Y_1^n | S_0}(\mathbf{x}_1^n, \mathbf{y}_1^n | \rho_{S_0}) \cdot \sum_k \sum_{s', s, \tilde{s}', \tilde{s}} \bar{\varrho}_{\hat{S}_{k-1}}^{(\mathbf{x}_1^{k-1}, \mathbf{y}_1^{k-1})}(s, \tilde{s}) \cdot H^{y_k|x_k}(s', s, \tilde{s}', \tilde{s}) \cdot \bar{\varrho}_{\hat{S}_k}^{(\mathbf{x}_{k+1}^n, \mathbf{y}_{k+1}^n)}(s', \tilde{s}') \quad (85)$$

$$\frac{d}{dt} \Big|_{t=0} \Delta^{(n)}(\hat{W} + tH) \propto -\frac{1}{n} \left\langle \sum_{k=1}^n \text{tr}([\hat{W}^{Y_n|X_n}] \dots [\hat{W}^{Y_{k+1}|X_{k+1}}][H^{Y_k|X_k}][\hat{W}^{Y_{k-1}|X_{k-1}}] \dots [\hat{W}^{Y_1|X_1}] \cdot [\rho_{\hat{S}_0}]) \right\rangle \quad (85)$$

$$= -\frac{1}{n} \sum_{\mathbf{x}_1^n, \mathbf{y}_1^n} P_{X_1^n, Y_1^n | S_0}(\mathbf{x}_1^n, \mathbf{y}_1^n | \rho_{S_0}) \cdot \sum_k \sum_{s', s, \tilde{s}', \tilde{s}} \bar{\varrho}_{\hat{S}_{k-1}}^{(\mathbf{x}_1^{k-1}, \mathbf{y}_1^{k-1})}(s, \tilde{s}) \cdot H^{y_k|x_k}(s', s, \tilde{s}', \tilde{s}) \cdot \bar{\varrho}_{\hat{S}_k}^{(\mathbf{x}_{k+1}^n, \mathbf{y}_{k+1}^n)}(s', \tilde{s}') \quad (86)$$

a fixed dimension (which can be different from the memory dimension of the original channel). We also consider the problem of optimizing the bounds and the difference between the upper and lower bounds over this domain. Throughout this section, we assume the original channel as described in Section III is indecomposable, that all the involved Hilbert spaces are of finite dimension, and that the alphabets \mathcal{X} and \mathcal{Y} are finite.

Suppose we have some auxiliary CC-QSC $\{\mathcal{N}^{y|x}\}_{x,y}$, describable by some functions $\{\hat{W}^{y|x}\}_{x,y}$ as in (48). Let $\hat{P}_{Y_1^n|X_1^n, \hat{S}_0}$ denote its joint channel law, similar to (40), (45) and (51). We follow the similar approach as in [12], [13], and define the following quantities:

$$\bar{\mathbb{I}}^{(n)}(\hat{W}) \triangleq \frac{1}{n} \left\langle \log \frac{P_{Y_1^n|X_1^n, S_0}(Y_1^n|X_1^n; \rho_{S_0})}{\sum_{\mathbf{x}_1^n} Q^{(n)}(\mathbf{x}_1^n) \hat{P}_{Y_1^n|X_1^n, \hat{S}_0}(Y_1^n|\mathbf{x}_1^n; \rho_{\hat{S}_0})} \right\rangle, \quad (87)$$

$$\underline{\mathbb{I}}^{(n)}(\hat{W}) \triangleq \frac{1}{n} \left\langle \log \frac{\hat{P}_{Y_1^n|X_1^n, \hat{S}_0}(Y_1^n|X_1^n; \rho_{\hat{S}_0})}{\sum_{\mathbf{x}_1^n} Q^{(n)}(\mathbf{x}_1^n) \hat{P}_{Y_1^n|X_1^n, \hat{S}_0}(Y_1^n|\mathbf{x}_1^n; \rho_{\hat{S}_0})} \right\rangle, \quad (88)$$

where $\langle \cdot \rangle$ is the expectation operator w.r.t. the joint distribution on (X_1^n, Y_1^n) as in (61). It is straightforward to verify the

inequalities

$$\underline{\mathbb{I}}^{(n)}(\hat{W}) \leq \bar{\mathbb{I}}^{(n)}(\hat{W}) \leq \bar{\mathbb{I}}^{(n)}(W), \quad (89)$$

where the first inequality holds with equality if and only if $\hat{P}_{Y_1^n|X_1^n, \hat{S}_0}(\mathbf{y}_1^n|\mathbf{x}_1^n; \rho_{\hat{S}_0})$ and $P_{Y_1^n|X_1^n, S_0}(\mathbf{y}_1^n|\mathbf{x}_1^n; \rho_{S_0})$ coincide for all \mathbf{x}_1^n and \mathbf{y}_1^n with positive support, and where the second inequality holds with equality if and only if $\hat{P}_{Y_1^n|\hat{S}_0}(\mathbf{y}_1^n|\rho_{\hat{S}_0})$ and $P_{Y_1^n|S_0}(\mathbf{y}_1^n|\rho_{S_0})$ coincide for all \mathbf{y}_1^n with positive support. Another quantity of interest is the *difference function* defined as

$$\Delta^{(n)}(\hat{W}) \triangleq \bar{\mathbb{I}}^{(n)}(\hat{W}) - \underline{\mathbb{I}}^{(n)}(\hat{W}). \quad (90)$$

Explicit expressions of (87), (88), and (90) can be found at the top of this page.

In the remainder of this Section, we propose an algorithm based on the gradient-descent method and the techniques described in Section III-C and IV for optimizing the quantities in (87), (88), and (90). In particular, we consider $\{\hat{W}^{y|x}\}_{x,y}$ to be an *interior* point in the domain of CC-QSCs, namely

- $\llbracket \hat{W}^{y|x} \rrbracket$ is strictly positive definite for each x and y ,
- Equation (60) holds by replacing $W^{y|x}$ with $\hat{W}^{y|x}$.

Algorithm 10 Estimating the information rate of a CC-QSC

Input: indecomposable CC-QSC $\{\mathcal{N}^{y|x}\}_{x \in \mathcal{X}, y \in \mathcal{Y}}$, which can be represented by functions $\{W^{y|x}\}_{x,y}$, input distribution Q , large positive integer n .

Output: $I^{(n)}(Q, \{\mathcal{N}^{y|x}\}_{x,y}) \approx \mathbf{H}(X) + \hat{\mathbf{H}}(Y) - \hat{\mathbf{H}}(X, Y)$.

- 1: Initialize the memory density operator $\rho_{S_0} \leftarrow |0_S\rangle\langle 0_S|$
 - 2: Generate an input sequence $\tilde{x}_1^n \sim Q^{\otimes n}$
 - 3: Generate a corresponding output sequence \tilde{y}_1^n
 - 4: $\bar{\sigma}_0^Y \leftarrow \rho_{S_0}$
 - 5: **for each** $\ell = 1, \dots, n$ **do**
 - 6: $[\sigma_\ell^Y] \leftarrow \sum_{x_\ell} Q(x_\ell) \cdot [W^{\tilde{y}_\ell|x_\ell}] \cdot [\bar{\sigma}_{\ell-1}^Y]$
 - 7: $\lambda_\ell^Y \leftarrow \text{tr}(\sigma_\ell^Y)$
 - 8: $\bar{\sigma}_\ell^Y \leftarrow \sigma_\ell^Y / \lambda_\ell^Y$
 - 9: **end for**
 - 10: $\hat{\mathbf{H}}(Y) \leftarrow -\frac{1}{n} \sum_{\ell=1}^n \log(\lambda_\ell^Y)$
 - 11: $\bar{\sigma}_0^{XY} \leftarrow \rho_{S_0}$
 - 12: **for each** $\ell = 1, \dots, n$ **do**
 - 13: $[\sigma_\ell^{XY}] \leftarrow [W^{\tilde{y}_\ell|\tilde{x}_\ell}] \cdot [\bar{\sigma}_{\ell-1}^{XY}]$
 - 14: $\lambda_\ell^{XY} \leftarrow \text{tr}(\sigma_\ell^{XY})$
 - 15: $\bar{\sigma}_\ell^{XY} \leftarrow \sigma_\ell^{XY} / \lambda_\ell^{XY}$
 - 16: **end for**
 - 17: $\hat{\mathbf{H}}(X, Y) \leftarrow -\frac{1}{n} \sum_{\ell=1}^n \log(\lambda_\ell^{XY})$
 - 18: $\mathbf{H}(X) \leftarrow -\sum_x Q(x) \log Q(x)$
 - 19: Estimate $I^{(n)}(Q, \{\mathcal{N}^{y|x}\}_{x,y})$ as $\mathbf{H}(X) + \hat{\mathbf{H}}(Y) - \hat{\mathbf{H}}(X, Y)$.
-

For any set of functions $\{H^{y|x}\}_{x,y}$ such that $\llbracket H^{y|x} \rrbracket$ is Hermitian for each x and y , and such that

$$\sum_{y \in \mathcal{Y}} \sum_{s', \bar{s}': s' = \bar{s}'} \llbracket H^{y|x} \rrbracket_{(s', s), (\bar{s}', \bar{s})} = 0 \quad \forall x \in \mathcal{X}, \quad (91)$$

the functions $\{\hat{W}^{y|x} + t \cdot H^{y|x}\}_{x,y}$ describe a valid CC-QSC, for all t in some neighborhood of 0. In this case, the directional derivatives of functions $\underline{I}^{(n)}$, $\bar{I}^{(n)}$, and $\Delta^{(n)}$ at $\{\hat{W}^{y|x}\}_{x,y}$ along $\{H^{y|x}\}_{x,y}$ is well-defined, and can be computed as shown in (81), (83), and (85), respectively.

By extending the domain of the functions $\underline{I}^{(n)}$, $\bar{I}^{(n)}$, and $\Delta^{(n)}$ to include *all* p.s.d. matrices $\llbracket \hat{W}^{y|x} \rrbracket$, one can omit the linear constraint (91). Namely, the ‘‘direction’’ $\llbracket H^{y|x} \rrbracket$ can be any Hermitian matrix. Observe that (81), (83), and (85) can be rewritten as (82), (84), and (86), respectively, where we define the messages

$$[\underline{\varrho}_{S_\ell}^{\tilde{y}_1^\ell}] \triangleq \sum_{x_1^\ell} Q(x_1^\ell) \cdot [\hat{W}^{\tilde{y}_\ell|x_\ell}] \cdots [\hat{W}^{\tilde{y}_1|x_1}] \cdot [\rho_{S_0}], \quad (92)$$

$$[\underline{\varrho}_{S_\ell}^{\tilde{y}_{\ell+1}^n}] \triangleq \sum_{x_{\ell+1}^n} Q(x_{\ell+1}^n) \cdot [I_{S_n}] \cdot [\hat{W}^{\tilde{y}_n|x_n}] \cdots [\hat{W}^{\tilde{y}_{\ell+1}|x_{\ell+1}}], \quad (93)$$

$$[\underline{\varrho}_{S_\ell}^{\tilde{x}_1^\ell, \tilde{y}_1^\ell}] \triangleq [\hat{W}^{\tilde{y}_\ell|\tilde{x}_\ell}] \cdots [\hat{W}^{\tilde{y}_1|\tilde{x}_1}] \cdot [\rho_{S_0}], \quad (94)$$

$$[\underline{\varrho}_{S_\ell}^{\tilde{x}_{\ell+1}^n, \tilde{y}_{\ell+1}^n}] \triangleq [I_{S_n}] \cdot [\hat{W}^{\tilde{y}_n|\tilde{x}_n}] \cdots [\hat{W}^{\tilde{y}_{\ell+1}|\tilde{x}_{\ell+1}}]. \quad (95)$$

Using some linear algebra, gradient w.r.t \hat{W} of these functions

on the extended domain can be expressed as

$$(\nabla \bar{I}_E^{(n)}(\hat{W}))^{y|x} \propto -\frac{1}{n} \left\langle \sum_{\substack{k: X_k=x \\ \wedge Y_k=y}} \underline{\varrho}_{S_{k-1}}^{(Y_1^{k-1})} \otimes \underline{\varrho}_{S_k}^{(Y_{k+1}^n)} \right\rangle, \quad (96)$$

$$(\nabla \Delta_E^{(n)}(\hat{W}))^{y|x} \propto -\frac{1}{n} \left\langle \sum_{\substack{k: X_k=x \\ \wedge Y_k=y}} \underline{\varrho}_{S_{k-1}}^{(X_1^{k-1}, Y_1^{k-1})} \otimes \underline{\varrho}_{S_k}^{(X_{k+1}^n, Y_{k+1}^n)} \right\rangle, \quad (97)$$

$$\nabla \underline{I}_E^{(n)}(\hat{W}) = \nabla \bar{I}_E^{(n)}(\hat{W}) - \nabla \Delta_E^{(n)}(\hat{W}). \quad (98)$$

For stationary and ergodic input and output processes (X_1^n, Y_1^n) , we can estimate (96) and (97) via

$$\begin{aligned} (\nabla \bar{I}_E^{(n)}(\hat{W}))^{y|x} &\propto -\frac{1}{n} \sum_{\substack{k: \tilde{x}_k=x \\ \wedge \tilde{y}_k=y}} \underline{\varrho}_{S_{k-1}}^{\tilde{y}_1^{k-1}} \otimes \underline{\varrho}_{S_k}^{\tilde{y}_{k+1}^n} \\ (\nabla \Delta_E^{(n)}(\hat{W}))^{y|x} &\propto -\frac{1}{n} \sum_{\substack{k: \tilde{x}_k=x \\ \wedge \tilde{y}_k=y}} \underline{\varrho}_{S_{k-1}}^{\tilde{x}_1^{k-1}, \tilde{y}_1^{k-1}} \otimes \underline{\varrho}_{S_k}^{\tilde{x}_{k+1}^n, \tilde{y}_{k+1}^n} \end{aligned} \quad (99)$$

where $(\tilde{x}_1^n, \tilde{y}_1^n)$ are some realization of the channel input and output processes generated by the original channel model. Notice that the messages $\underline{\varrho}_{S_{k-1}}^{\tilde{y}_1^{k-1}}$, $\underline{\varrho}_{S_k}^{\tilde{y}_{k+1}^n}$, $\underline{\varrho}_{S_{k-1}}^{\tilde{x}_1^{k-1}, \tilde{y}_1^{k-1}}$, and $\underline{\varrho}_{S_k}^{\tilde{x}_{k+1}^n, \tilde{y}_{k+1}^n}$ can be computed iteratively. Thus, (99) and (100) provide efficient means to estimate the gradient. However, due to the extension of the domain, the gradients computed above may not satisfy constraint (91). This can be compensated using a projection w.r.t. the linear constraint, which can be solved using linear programming. On the other hand, the above gradient method may lead to a violation of the p.s.d. condition required by CC-QSCs. However, since the feasible domain of CC-QSCs is convex and bounded, this can be corrected using convex programming.

We summarize the above discussion as Algorithm 11, which is an iterative gradient-descent method for minimizing $\Delta^{(n)}$. The algorithm for minimizing the upper and lower bounds are similar, and we omit the details.

VI. EXAMPLE: QUANTUM GILBERT–ELLIOTT CHANNELS

In this section we present some numerical results as a demonstration of the algorithms introduced in this paper. In particular, we consider a class of quantum channels with memory named the quantum Gilbert–Elliott channels (QGECs) introduced in [1], and consider its information rate using some separable ensemble and local measurement.

A QGEC is a quantum channel with memory defined by

$$\begin{aligned} \mathcal{N} : \mathfrak{D}(\mathcal{H}_S \otimes \mathcal{H}_A) &\rightarrow \mathfrak{D}(\mathcal{H}_{S'} \otimes \mathcal{H}_B) \\ \rho_{SA} &\mapsto (U_S \otimes I_B) \cdot \Phi^{\text{GE}}(\rho_{SA}) \cdot (U_S^H \otimes I_B), \end{aligned}$$

where

- $\mathcal{H}_A, \mathcal{H}_B$, and $\mathcal{H}_S = \mathcal{H}_{S'}$ are of dimension 2, namely each of them is made up of one qubit;
- Φ^{GE} is a CPTP map defined as

$$\Phi^{\text{GE}}(\rho_{SA}) = E_0 \rho^{\text{SA}} E_0^H + E_1 \rho^{\text{SA}} E_1^H$$

Algorithm 11 Optimizing the difference function

Input: indecomposable CC-QSC,
input distribution Q ,
large positive integer n ,
initial auxiliary CC-QSC $\{\hat{W}^{y|x}\}_{x,y}$
descent coefficient $\gamma > 0$.

Output: $\{\hat{W}^{y|x}\}_{x,y}$, a local minimum point of $\Delta^{(n)}$.

- 1: Initialize the memory density operator $\rho_{\mathcal{S}_0} \leftarrow |0\rangle\langle 0|$
- 2: Generate an input sequence $\tilde{x}_1^n \sim Q^{\otimes n}$
- 3: Generate a corresponding output sequence \tilde{y}_1^n
- 4: **repeat**
- 5: $\tilde{\varrho}_{\mathcal{S}_0} \leftarrow \rho_{\mathcal{S}_0}$
- 6: **for each** $\ell = 1, \dots, n$ **do**
- 7: $[\tilde{\varrho}_{\mathcal{S}_\ell}] \leftarrow [\hat{W}^{\tilde{y}_\ell|\tilde{x}_\ell}] \cdot [\tilde{\varrho}_{\mathcal{S}_{\ell-1}}]$
- 8: $\lambda_\ell \leftarrow \text{tr}(\tilde{\varrho}_{\mathcal{S}_\ell})$
- 9: $\tilde{\varrho}_{\mathcal{S}_\ell} \leftarrow \lambda_\ell^{-1} \cdot \tilde{\varrho}_{\mathcal{S}_\ell}$
- 10: **end for**
- 11: $\tilde{\varrho}_{\mathcal{S}_n} \leftarrow I_{\mathcal{S}_n}$
- 12: **for each** $\ell = n, \dots, 1$ **do**
- 13: $[\tilde{\varrho}_{\mathcal{S}_{\ell-1}}] \leftarrow [\tilde{\varrho}_{\mathcal{S}_\ell}] \cdot [\hat{W}^{\tilde{y}_\ell|\tilde{x}_\ell}]$
- 14: $\tilde{\varrho}_{\mathcal{S}_{\ell-1}} \leftarrow \left(\text{tr}(\tilde{\varrho}_{\mathcal{S}_{\ell-1}})\right)^{-1} \cdot \tilde{\varrho}_{\mathcal{S}_{\ell-1}}$
- 15: **end for**
- 16: for each x, y , let $\left(\nabla \Delta_E^{(n)}(\hat{W})\right)^{y|x} \leftarrow \mathbf{0}$
- 17: **for each** $k = 1, \dots, n$ **do**
- 18: $\left(\nabla \Delta_E^{(n)}(\hat{W})\right)^{y_k|\tilde{x}_k} += \frac{1}{n} \cdot \frac{\tilde{\varrho}_{\mathcal{S}_{k-1}} \otimes \tilde{\varrho}_{\mathcal{S}_k}}{\lambda_k \cdot \text{tr}(\tilde{\varrho}_{\mathcal{S}_k} \cdot \tilde{\varrho}_{\mathcal{S}_k})}$
- 19: **end for**
- 20: Project $\left\{\left(\nabla \Delta_E^{(n)}(\hat{W})\right)^{y|x}\right\}_{x,y}$ onto the subspace satisfying $\sum_y \sum_{s', \bar{s}'}: s'=\bar{s}' \llbracket (\nabla \Delta^{(n)})^{y|x} \rrbracket = 0$ for all x ; and denote the result as $\left\{\left(\nabla \Delta^{(n)}(\hat{W})\right)^{y|x}\right\}_{x,y}$
- 21: $\{\hat{W}^{y|x}\}_{x,y} \leftarrow \{\hat{W}^{y|x}\}_{x,y} - \gamma \cdot \left\{\left(\nabla \Delta^{(n)}(\hat{W})\right)^{y|x}\right\}_{x,y}$
- 22: Solve the following convex program w.r.t. $\{\hat{W}^{y|x}\}_{x,y}$:
$$\begin{aligned} \min & \sum_{x,y} \text{tr} \left(\left(\llbracket \hat{W}^{y|x} \rrbracket - \llbracket \hat{W}^{y|x} \rrbracket \right) \left(\llbracket \hat{W}^{y|x} \rrbracket - \llbracket \hat{W}^{y|x} \rrbracket \right)^H \right) \\ \text{s.t.} & \llbracket \hat{W}^{y|x} \rrbracket \in \mathbb{C}^{\mathcal{S}^2 \times \mathcal{S}^2} \text{ is p.s.d. for each } x, y \\ & \sum_{y \in \mathcal{Y}} \sum_{s', \bar{s}': s'=\bar{s}'} \llbracket \hat{W}^{y|x} \rrbracket_{(s',s),(\bar{s}',\bar{s})} = \delta_{s,\bar{s}} \quad \forall x \end{aligned}$$
- 23: $\{\hat{W}^{y|x}\} \leftarrow \{\hat{W}^{y|x}\}$
- 24: **until** $\{\hat{W}^{y|x}\}_{x,y}$ has converged.

where

$$E_0 \triangleq \begin{bmatrix} \sqrt{1-p_g} & 0 & 0 & 0 \\ 0 & \sqrt{1-p_g} & 0 & 0 \\ 0 & 0 & \sqrt{1-p_b} & 0 \\ 0 & 0 & 0 & \sqrt{1-p_b} \end{bmatrix}, \quad E_1 \triangleq \begin{bmatrix} 0 & \sqrt{p_g} & 0 & 0 \\ \sqrt{p_g} & 0 & 0 & 0 \\ 0 & 0 & 0 & \sqrt{p_b} \\ 0 & 0 & \sqrt{p_b} & 0 \end{bmatrix}.$$

- $U_{\mathcal{S}}$ is some unitary operator on $\mathcal{H}_{\mathcal{S}}$.

We choose ensemble and measurements to be

$$\begin{aligned} \rho_A^x &\triangleq |x\rangle\langle x| & \forall x \in \mathcal{X} = \{0, 1\}, \\ \Lambda_B^x &\triangleq |y\rangle\langle y| & \forall y \in \mathcal{Y} = \{0, 1\}. \end{aligned}$$

In this case, the induced CC-QSC $\{\mathcal{N}^{y|x}\}_{x,y}$ can be expressed as

$$\mathcal{N}^{y|x}(\rho_S) = \text{tr}_B \left((U_S^H U_S \otimes |y\rangle\langle y|) \Phi^{\text{GE}}(\rho_S \otimes |x\rangle\langle x|) \right) \quad \forall x, y.$$

In Figs. 10–13, we present some numerical information rate lower bounds estimated for various setups of the QGEC, where the channel input process is a binary symmetric i.i.d. process. The lower bounds were obtained by minimizing the difference function $\Delta^{(n)}$ defined in (29) with respect to different classes of auxiliary channels (subject to certain time and threshold constrains). For the case where the auxiliary channels are CC-QSCs, the methods described in Section V were applied. For other types of auxiliary channels, please see the figure captions for further details. As already emphasized beforehand, these lower bounds represent rates that are achievable with the help of a mismatched decoder [17]. Fig. 9 is an example illustrating the typical convergence time of different methods (including our own) for minimizing the difference function.

VII. CONCLUSION

In this article, we considered the scenario of transmitting classical information over a quantum channel with finite memory using separable-state ensembles and local measurements. We defined the notion of CC-QSCs as an equivalent way to describe such communication setups, and demonstrated how NFGs can be used to visualize such channels. We showed that the information rate of a quantum-state channel is independent of the initial density operator under suitable conditions, and proposed algorithms for estimating and bounding such information rate. The computations in such algorithms can be carried out using the corresponding NFGs of the CC-QSC. We emphasize that our approach for optimizing the lower bound is data-driven, and does not require the knowledge of the true channel model.

ACKNOWLEDGMENT

It is a great pleasure to acknowledge discussions on topics related to this paper with Andi Loeliger.

REFERENCES

- [1] M. X. Cao and P. O. Vontobel, “Estimating the information rate of a channel with classical input and output and a quantum state,” in *Proc. IEEE Int. Symp. Inf. Theory*, Jun. 2017, pp. 3205–3209.
- [2] G. Bowen and S. Mancini, “Quantum channels with a finite memory,” *Phys. Rev. A*, vol. 69, no. 1, p. 012306, 2004.
- [3] D. Kretschmann and R. F. Werner, “Quantum channels with memory,” *Phys. Rev. A*, vol. 72, no. 6, p. 062323, 2005.
- [4] F. Caruso, V. Giovannetti, C. Lupo, and S. Mancini, “Quantum channels and memory effects,” *Rev. Mod. Phys.*, vol. 86, no. 4, p. 1203, 2014.
- [5] M. A. Nielsen and I. L. Chuang, *Quantum Computation and Quantum Information*, 10th Anniversary ed. Cambridge University Press, 2011.
- [6] M. M. Wilde, *Quantum Information Theory*, 2nd ed. Cambridge University Press, 2017.
- [7] S. Bose, “Quantum communication through an unmodulated spin chain,” *Phys. Rev. Lett.*, vol. 91, no. 20, p. 207901, 2003.
- [8] J. Ball, A. Dragan, and K. Banaszek, “Exploiting entanglement in communication channels with correlated noise,” *Phys. Rev. A*, vol. 69, no. 4, p. 042324, 2004.
- [9] C. E. Shannon, “A mathematical theory of communication,” *Bell System Technical Journal*, vol. 27, no. 3, pp. 379–423, 1948.
- [10] T. M. Cover and J. A. Thomas, *Elements of Information Theory*, 2nd ed. John Wiley & Sons, 2006.

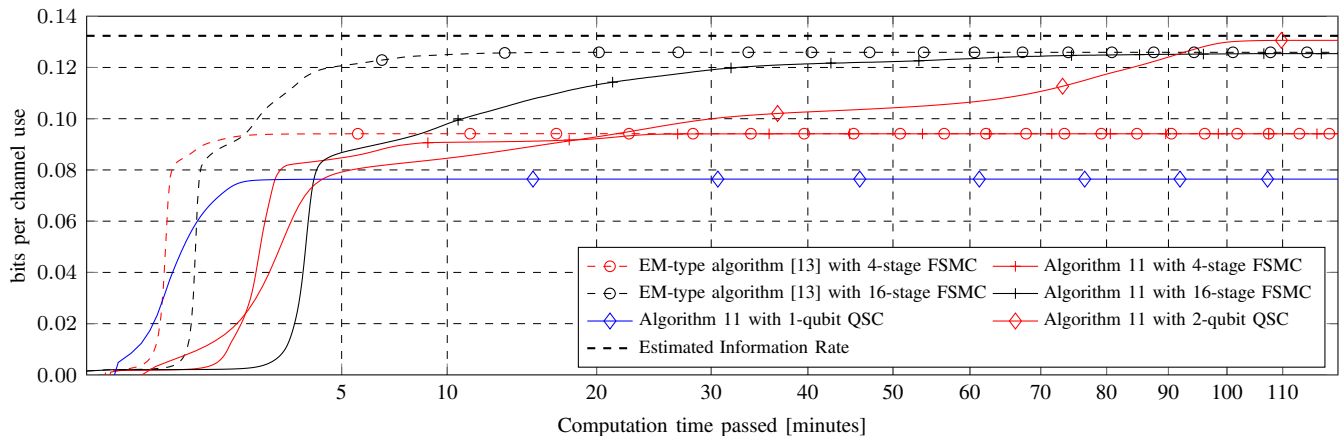


Fig. 9: Minimizing the difference function $\Delta^{(n)}$ using different methods. The markers appear after every 400 updates.

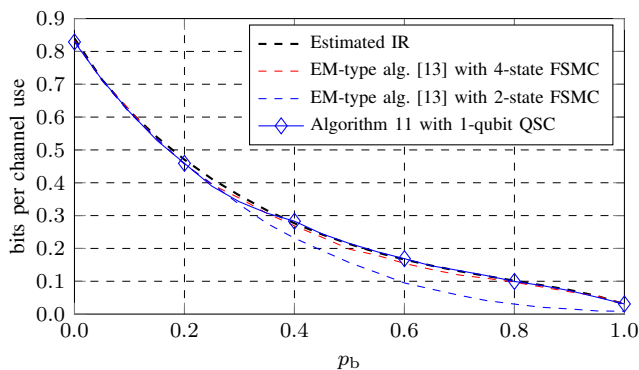


Fig. 10: Quantum Gilbert–Elliott Channel: $p_g = 0.05$ is fixed; p_b varies from 0 to 1; $U = \exp(-i\alpha H)$, where H is some fixed Hermitian matrix and where $\alpha = 1$ is fixed; $n = 10^5$.

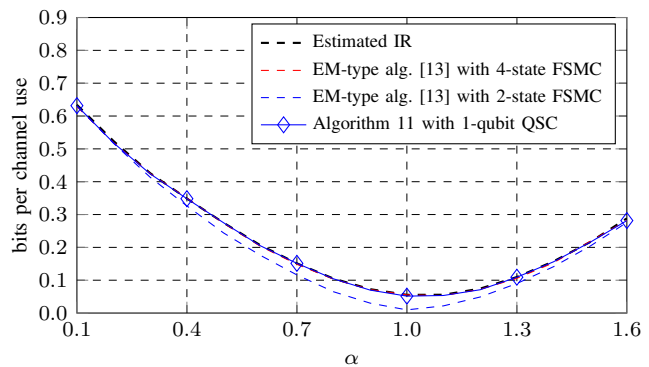


Fig. 12: Quantum Gilbert–Elliott Channel: $p_g = 0.05$ is fixed; $p_b = 0.95$ is fixed; $U = \exp(-i\alpha H)$, where H is the same Hermitian matrix as in Fig. 10 and where α varies from -1.5 to $+1.5$; $n = 10^5$. (No information rate estimates are included for α around 0 because of slow mixing of the channel.)

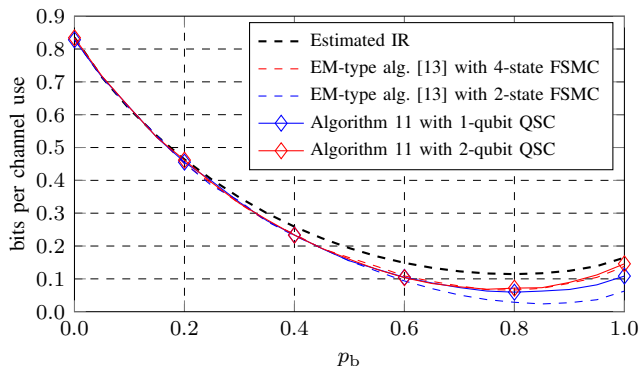


Fig. 11: Variant of the Quantum Gilbert–Elliott Channel where the state quantum system consists of two qubits whose evolution is described by U , but where only one of the qubits interacts directly with the transmit quantum system: $p_g = 0.05$ is fixed; p_b varies from 0 to 1; $U = \exp(-j\alpha H)$, where H is some fixed Hermitian matrix and where $\alpha = 1$ is fixed; $n = 10^5$.

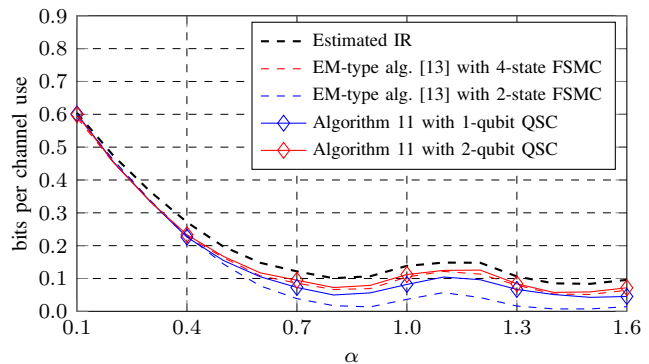


Fig. 13: Same variant of the Quantum Gilbert–Elliott Channel as in Fig. 11: $p_g = 0.05$ is fixed; $p_b = 0.95$ is fixed; $U = \exp(-i\alpha H)$, where H is the same Hermitian matrix as in Fig. 11 and where α varies from -1.5 to $+1.5$; $n = 10^5$. (No information rate estimates are included for α around 0 because of slow mixing of the channel.)

- [11] R. G. Gallager, *Information Theory and Reliable Communication*, 1st ed. Wiley, 1968.
- [12] D.-M. Arnold, H.-A. Loeliger, P. O. Vontobel, A. Kavčić, and W. Zeng, "Simulation-based computation of information rates for channels with memory," *IEEE Trans. Inf. Theory*, vol. 52, no. 8, pp. 3498–3508, 2006.
- [13] P. Sadeghi, P. O. Vontobel, and R. Shams, "Optimization of information rate upper and lower bounds for channels with memory," *IEEE Trans. Inf. Theory*, vol. 55, no. 2, pp. 663–688, 2009.
- [14] V. Sharma and S. Singh, "Entropy and channel capacity in the regenerative setup with applications to Markov channels," in *Proc. IEEE Int. Symp. Inf. Theory*, Jun. 2001, p. 283.
- [15] H. D. Pfister, J. B. Soriaga, and P. H. Siegel, "On the achievable information rates of finite state ISI channels," in *Proc. IEEE Global Telecom. Conf.*, vol. 5, Nov. 2001, pp. 2992–2996.
- [16] H.-A. Loeliger and P. O. Vontobel, "Factor graphs for quantum probabilities," *IEEE Trans. Inf. Theory*, vol. 63, no. 9, pp. 5642–5665, 2017.
- [17] A. Ganti, A. Lapidoth, and I. E. Telatar, "Mismatched decoding revisited: General alphabets, channels with memory, and the wide-band limit," *IEEE Trans. Inf. Theory*, vol. 46, no. 7, pp. 2315–2328, 2000.
- [18] S. Arimoto, "An algorithm for computing the capacity of arbitrary discrete memoryless channels," *IEEE Trans. Inf. Theory*, vol. 18, no. 1, pp. 14–20, 1972.
- [19] R. Blahut, "Computation of channel capacity and rate-distortion functions," *IEEE Trans. Inf. Theory*, vol. 18, no. 4, pp. 460–473, 1972.
- [20] P. O. Vontobel, A. Kavčić, D. M. Arnold, and H.-A. Loeliger, "A generalization of the Blahut–Arimoto algorithm to finite-state channels," *IEEE Trans. Inf. Theory*, vol. 54, no. 5, pp. 1887–1918, 2008.
- [21] M. B. Hastings, "Superadditivity of communication capacity using entangled inputs," *Nature Physics*, vol. 5, no. 4, p. 255, 2009.
- [22] C. Macchiavello, G. M. Palma, and S. Virmani, "Transition behavior in the channel capacity of two-qubit channels with memory," *Phys. Rev. A*, vol. 69, no. 1, p. 010303, 2004.
- [23] V. Karimipour and L. Memarzadeh, "Entanglement and optimal strings of qubits for memory channels," *Phys. Rev. A*, vol. 74, no. 6, p. 062311, 2006.
- [24] C. Lupo and S. Mancini, "Transitional behavior of quantum Gaussian memory channels," *Phys. Rev. A*, vol. 81, no. 5, p. 052314, 2010.
- [25] F. R. Kschischang, B. J. Frey, and H.-A. Loeliger, "Factor graphs and the sum-product algorithm," *IEEE Trans. Inf. Theory*, vol. 47, no. 2, pp. 498–519, 2001.
- [26] G. D. Forney, "Codes on graphs: Normal realizations," *IEEE Trans. Inf. Theory*, vol. 47, no. 2, pp. 520–548, 2001.
- [27] H.-A. Loeliger, "An introduction to factor graphs," *IEEE Signal Process. Mag.*, vol. 21, no. 1, pp. 28–41, 2004.
- [28] M. X. Cao and P. O. Vontobel, "Double-edge factor graphs: definition, properties, and examples," in *Proc. IEEE Inf. Theory Workshop*. IEEE, 2017, pp. 136–140.
- [29] M. Mushkin and I. Bar-David, "Capacity and coding for the Gilbert–Elliott channels," *IEEE Trans. Inf. Theory*, vol. 35, no. 6, pp. 1277–1290, 1989.
- [30] Y. Ephraim and N. Merhav, "Hidden Markov processes," *IEEE Trans. Inf. Theory*, vol. 48, no. 6, pp. 1518–1569, 2002.
- [31] G. Bowen, I. Devetak, and S. Mancini, "Bounds on classical information capacities for a class of quantum memory channels," *Phys. Rev. A*, vol. 71, no. 3, p. 034310, 2005.

APPENDIX

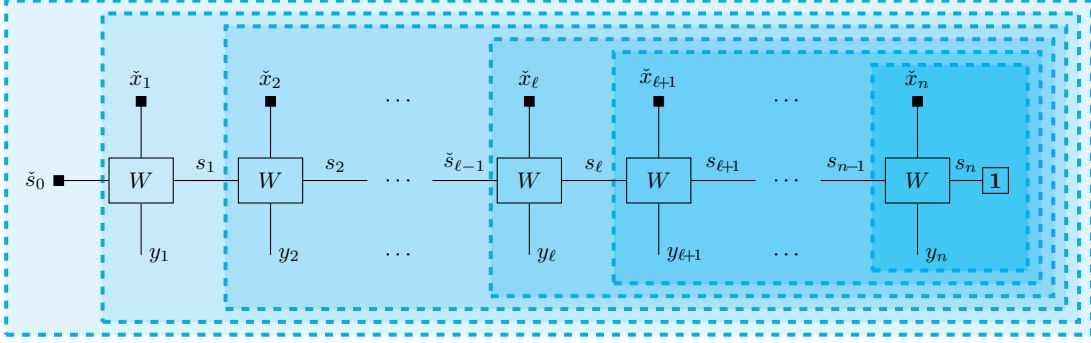


Fig. 14: Verification of (8). Note that every closing-the-box operation yields a function node representing the constant function 1.

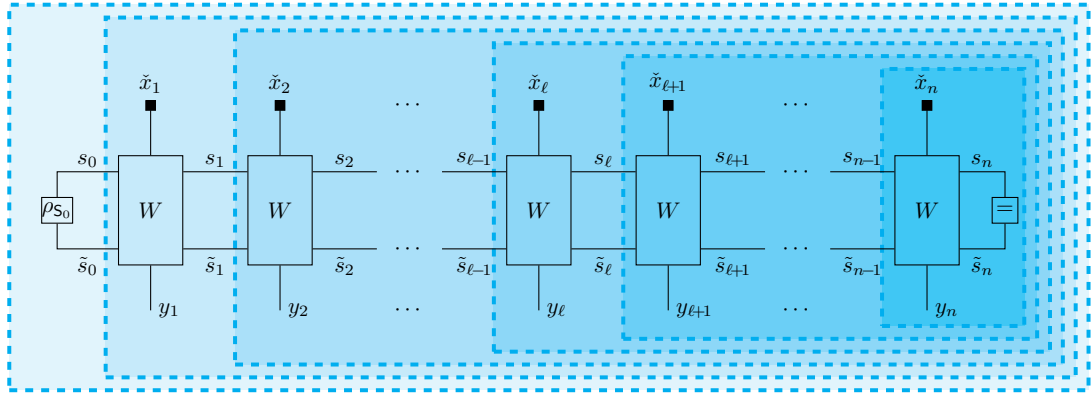


Fig. 15: Counterpart of Fig. 14 for QSCs. Note that every closing-the-box operation yields a function node representing a Kronecker-delta function node, i.e., a degree-two equality function node.

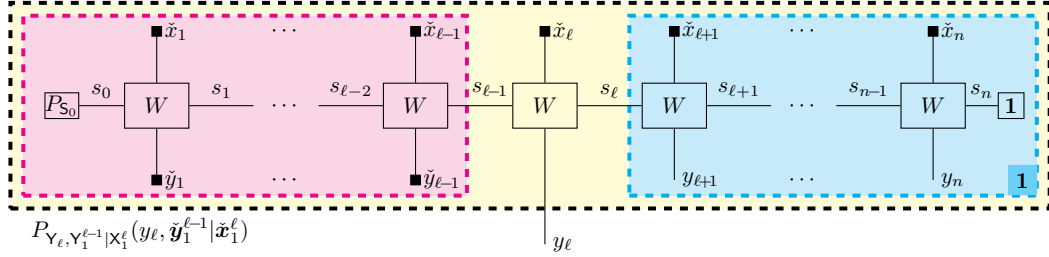


Fig. 16: Efficient simulation of the channel output at step ℓ given channel input \tilde{x}_1^n and channel output $\tilde{y}_1^{\ell-1}$ for an FSMC.

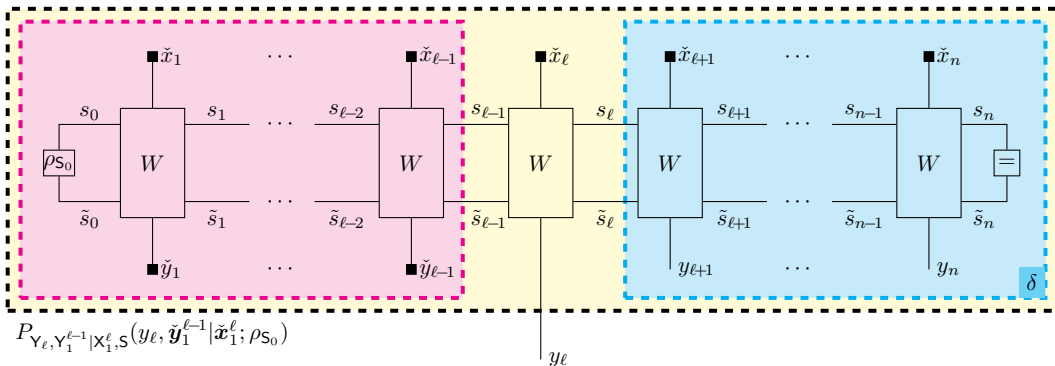


Fig. 17: Efficient simulation of the channel output at step ℓ given channel input \tilde{x}_1^n and channel output $\tilde{y}_1^{\ell-1}$ for a QSC.

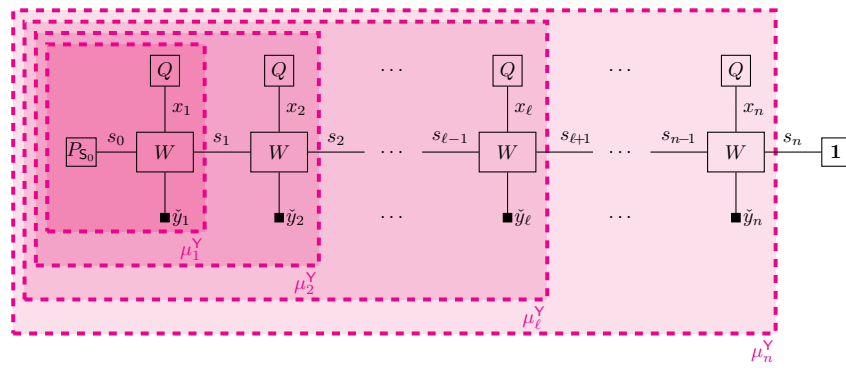


Fig. 18: The iterative computation of μ_ℓ^Y as in (21) can be understood as a sequence of CTB operations as shown above.

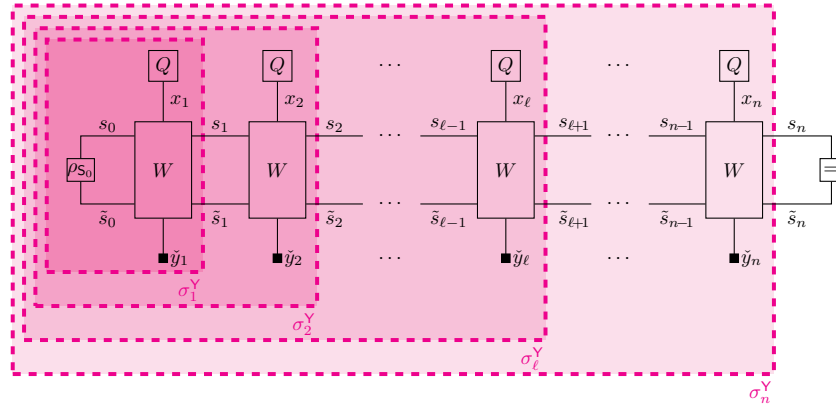


Fig. 19: The iterative computation of σ_ℓ^Y as in (76) can be understood as a sequence of CTB operations as shown above.

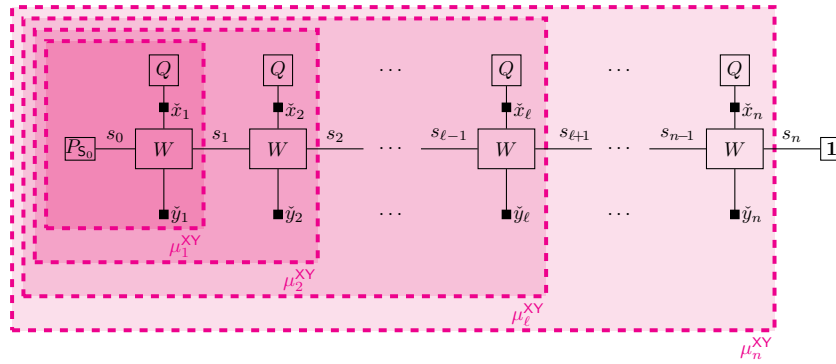


Fig. 20: The iterative computation of μ_ℓ^{XY} can be understood as a sequence of CTB operations as shown above.

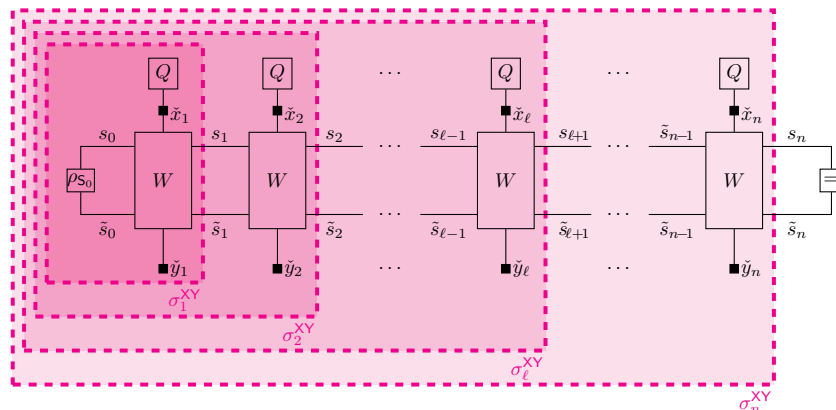


Fig. 21: The iterative computation of σ_ℓ^{XY} as in (77) can be understood as a sequence of CTB operations as shown above.